A&A, 684, A84 (2024)
https://doi.org/10.1051/0004-6361/202347132
© The Authors 2024

Astronomy & Astrophysics

JADES: The production and escape of ionizing photons from faint Lyman-alpha emitters in the epoch of reionization

Aayush Saxena[1,2], Andrew J. Bunker[1], Gareth C. Jones[1], Daniel P. Stark[3], Alex J. Cameron[1], Joris Witstok[4,5], Santiago Arribas[6], William M. Baker[4,5], Stefi Baum[7], Rachana Bhatawdekar[8,9], Rebecca Bowler[10], Kristan Boyett[11,12], Stefano Carniani[13], Stephane Charlot[14], Jacopo Chevallard[1], Mirko Curti[15,4,5], Emma Curtis-Lake[16], Daniel J. Eisenstein[17], Ryan Endsley[18], Kevin Hainline[3], Jakob M. Helton[3], Benjamin D. Johnson[17], Nimisha Kumari[19], Tobias J. Looser[4,5], Roberto Maiolino[4,5,2], Marcia Rieke[3], Hans-Walter Rix[20], Brant E. Robertson[21], Lester Sandles[4,5], Charlotte Simmonds[4,5], Renske Smit[22], Sandro Tacchella[4,5], Christina C. Williams[23], Christopher N. A. Willmer[3], and Chris Willott[24]

(Affiliations can be found after the references)

Received 8 June 2023 / Accepted 25 January 2024

ABSTRACT

We present the properties of 17 faint Lyman-α emitting galaxies (LAEs) at $z > 5.8$ from the JWST Advanced Deep Extragalactic Survey (JADES) spectroscopic data in the *Hubble* Ultra Deep Field/GOODS-S. These LAEs span a redshift range $z \approx 5.8-8.0$ and a UV magnitude range $M_{\rm UV} \approx -17$ to -20.6, with the Lyα equivalent width (EW) in the range $\approx 25-350$ Å. The detection of other rest-optical emission lines in the spectra of these LAEs enables the determination of accurate systemic redshifts and Lyα velocity offsets, as well as the physical and chemical composition of their stars and interstellar media. These faint LAEs are consistent with metal-poor systems with high ionization parameters, similar to the general galaxy population at $z > 6$. We measured an average ionizing photon production efficiency, $\log(\xi_{\rm ion}/{\rm erg^{-1}\ Hz}) \approx 25.57$ across our LAEs, which does not evolve strongly with redshift. We report an anti-correlation between the Lyα escape fraction and the velocity offset from systemic redshift, consistent with model expectations. We further find that the strength and velocity offset of Lyα are neither correlated with galaxy spectroscopic properties nor with $\xi_{\rm ion}$. We find a decrease in Lyα escape fractions with redshift, indicative of decreasing sizes of ionized bubbles around LAEs at high redshifts. We used a range of galaxy properties to predict Lyman continuum escape fractions for our LAEs, finding that the ionizing photon output into the intergalactic medium from our LAEs remains roughly constant across the observed Lyα EW, showing a mild increase at fainter UV magnitudes and at higher redshifts. We derived correlations between the ionizing photon output from LAEs and their UV magnitudes, Lyα strengths and redshifts, which can be used to constrain the ionizing photon contribution of LAEs at $z > 6$ towards cosmic reionization.

Key words. galaxies: evolution – galaxies: high-redshift – galaxies: star formation – dark ages, reionization, first stars

1. Introduction

Cosmic reionization is a crucial phase transition in the Universe's history, and the understanding of which is an important challenge in observational astronomy (see recent review by Robertson 2022). The emergence of ionizing UV photons from the first structures to form in the Universe began interacting with the neutral intergalactic medium (IGM), gradually ionizing it to near completion by $z \sim 6$ (e.g. Fan et al. 2006), although certain studies have favoured a later end to reionization (e.g. Weinberger et al. 2019; Keating et al. 2020; Bosman et al. 2022). To quantify the contribution towards the cosmic reionization budget from ionizing photon sources in the early Universe, a good understanding is needed of the space density of sources, the efficiency of hydrogen ionizing Lyman continuum (LyC; $\lambda_0 < 912$ Å) photon production, and crucially, the fraction of LyC photons that manage to escape into the IGM (e.g. Dayal & Ferrara 2018).

JWST spectroscopy has offered ground-breaking insights into the state of the interstellar medium (ISM), chemical enrichment of the gas and stars as well as ionizing photon production in galaxies at $z > 6$, pushing towards fainter UV magnitudes than were previously possible from the ground (Arellano-Córdova et al. 2022; Endsley et al. 2023; Tacchella et al. 2023; Trump et al. 2023; Sun et al. 2023; Cameron et al. 2023; Curtis-Lake et al. 2023; Curti et al. 2023; Fujimoto et al. 2023; Katz et al. 2023a; Robertson et al. 2023; Sanders et al. 2023). However, accurately measuring the escape fraction of LyC photons ($f_{\rm esc}$) becomes hard already at $z > 4$ mainly due to the increasing neutrality of the IGM (e.g. Inoue et al. 2014), which efficiently absorbs LyC photons along the line of sight. A further complication is introduced by the fact that no clear dependence between $f_{\rm esc}$(LyC) and galaxy properties has been observationally established (e.g. Naidu et al. 2018; Fletcher et al. 2019; Nakajima et al. 2020; Pahl et al. 2021; Saxena et al. 2022b).

Therefore, in order to constrain the all-important escape fraction of ionizing photons from reionization era galaxies, it is of the utmost importance to find reliable indirect indicators of $f_{\rm esc}$(LyC). The presence of young, actively forming stars as well as gas and dust-free environments is thought to enable significant $f_{\rm esc}$(LyC) from galaxies (e.g. Zackrisson et al. 2013), and spectroscopic and/or photometric indicators probing such conditions can be explored as indirect indicators of LyC photon escape (e.g. Flury et al. 2022a,b; Topping et al. 2022; Mascia et al. 2023). Important insights can also be gained from high-resolution simulations of reionization era galaxies, where a good handle on the escaping LyC radiation can be correlated with prevalent galaxy conditions (e.g. Barrow et al. 2020; Maji et al. 2022) that can

Open Access article, published by EDP Sciences, under the terms of the Creative Commons Attribution License (https://creativecommons.org/licenses/by/4.0), which permits unrestricted use, distribution, and reproduction in any medium, provided the original work is properly cited.
This article is published in open access under the Subscribe to Open model. Subscribe to A&A to support open access publication.

then be converted into observables (e.g. Choustikov et al. 2024) and used to predict f_{esc} from galaxies.

Uniquely, galaxies at $z \gtrsim 6$ that show strong Lyα emission in their spectra, typically with equivalent widths (EW > 20 Å; e.g. Ajiki et al. 2003), also known as Lyα emitters (or LAEs) can be excellent probes of studying how reionization unfolds over redshifts. The presence of strong Lyα emission at $z \gtrsim 6$ often traces the existence of large ionized bubbles in an otherwise neutral IGM (Miralda-Escudé 1998; Furlanetto et al. 2006; Roberts-Borsani et al. 2016; Castellano et al. 2022; Trapp et al. 2023; Tang et al. 2023; Jung et al. 2023; Saxena et al. 2023, cf. Bunker et al. 2023b), offering direct observational insights into reionized regions of the early Universe. Further, as intrinsic Lyα luminosities are expected to increase with star formation rates, the fraction of galaxies that appear to be strong LAEs can be an important diagnostic of the ionizing photon production capabilities of reionization era galaxies (e.g. Smith et al. 2019; Garel et al. 2021; Matthee et al. 2022) as well as the evolving state of the IGM neutral fraction (e.g. Caruana et al. 2012, 2014; Stark 2016; Pentericci et al. 2018a; Hoag et al. 2019; Kusakabe et al. 2020; Fuller et al. 2020; Jones et al. 2024).

Considerable information about the neutral gas and dust content within a galaxy can be gained by the observed strength and emission line profile of Lyα (e.g. Hayes et al. 2023). The separation between the blue and red peaks in the emission as well as the offset from systemic redshift in the absence of a double-peaked profile can be used to infer neutral gas densities (Verhamme et al. 2015; Orlitová et al. 2018) and dust (Hayes et al. 2013), although it has been shown that the neutral gas distribution may play the more dominant role in controlling Lyα escape (e.g. Atek et al. 2008). At $z > 6$, both the number density of LAEs (Haiman 2002; Malhotra & Rhoads 2006) and the shape of the Lyα line originating from star-forming galaxies residing within ionized bubbles can further be used to estimate the size of those bubbles (e.g. Mason & Gronke 2020; Hayes & Scarlata 2023; Witstok et al. 2024).

With a plethora of models available to link the observed Lyα properties to both galaxy properties and the state of the IGM at $z > 6$, it is imperative to expand samples of observed LAEs in the reionization era, pushing to fainter magnitudes. Probing Lyα emission from UV-faint galaxies has the added advantage of providing much tighter constraints on both bubble sizes as well as the ionized fraction of the IGM (e.g. Mason et al. 2018; Bolan et al. 2022). Importantly, Lyα emission from fainter galaxies can provide additional sightlines from which the impact of galaxy associations on the production efficiency of ionizing photons (e.g. Witten et al. 2024) and their transmission through the IGM (e.g. Trapp et al. 2023) can be studied in detail.

Perhaps most importantly, detailed studies of faint LAEs can inform our understanding of the key drivers of cosmic reionization, particularly testing whether compact star-forming galaxies are indeed contributing the bulk of ionizing photons towards the reionization budget (e.g. Robertson et al. 2015), which are often expected to produce large intrinsic Lyα luminosities (e.g. Matthee et al. 2022). LAEs that have their Lyα emission peaking close to systemic redshifts are also expected to have high LyC escape fractions (Verhamme et al. 2015; Dijkstra 2014; Naidu et al. 2022). With signatures of hard radiation fields (Stark et al. 2015; Mainali et al. 2017; Feltre et al. 2020; Saxena et al. 2022a; Roy et al. 2023) and elevated ionizing photon production efficiencies (e.g. Matthee et al. 2017a; Harikane et al. 2018; Ning et al. 2023; Simmonds et al. 2023, 2024) measured from LAEs across redshifts, Lyα emitting galaxies in the reionization era are exciting laboratories to both test and constrain reionization models. With access to stellar and ISM properties of LAEs at high redshifts thanks to JWST, it is now finally possible to study the potential role of LAEs in driving cosmic reionization.

In an attempt to quantify the production and escape of both Lyα and LyC photons from LAEs in the reionization era, in this study we dramatically increase the number of faint LAEs detected at $z \gtrsim 6$ using exquisitely deep spectra from the JWST Advanced Deep Extragalactic Survey (JADES; Eisenstein et al. 2023). The main aim of this work is to explore the physical properties of faint LAEs in the reionization era, while also investigating the physical mechanisms within the galaxy that control the visibility of Lyα emission. We further assess the impact of an increasingly neutral IGM on the emergent Lyα emission at the highest redshifts. Finally, using all available spectroscopic and photometric information about our faint LAEs, we estimate their ionizing photon contribution towards the global reionization budget. In companion papers, we also measure the LAE fraction (Jones et al. 2024) as well as the size of ionized bubbles around our LAEs and their clustering (Witstok et al. 2024).

The layout of this paper is as follows: Section 2 describes the JWST data used in this study as well as the measurement of key spectroscopic quantities that are used in this study. Section 3 presents the chemical enrichment and ionization state inferred from the spectra of our LAEs compared with other reionization era galaxies in the literature. Section 4 explores the mechanisms within galaxies that control the escape of Lyα photons along the line of sight. Section 5 discusses the implications for the reionization of the Universe from these new LAE observations and presents quantities that would help build realistic reionization models. The main conclusions of this study are presented in Sect. 6.

Throughout this paper, we use the Planck Collaboration VI (2020) cosmology. Magnitudes are in the AB system (Oke & Gunn 1983) and all distances used are proper distances, unless otherwise stated.

2. Data and measurements

2.1. NIRSpec data

The JWST observations used in this study are part of JADES, which is a collaboration between the Near-Infrared Camera (NIRCam; Rieke et al. 2023a) and Near-Infrared Spectrograph (NIRSpec; Ferruit et al. 2022; Jakobsen et al. 2022) Instrument Science teams with an aim of using over 750 hours of guaranteed time observations (GTO) to study the evolution of galaxies in the Great Observatories Origins Deep Survey (GOODS)-South and GOODS-North fields (Giavalisco et al. 2004). We describe the NIRSpec and NIRCam observations and data reduction steps below.

Spectroscopic data presented in this work was obtained using the Micro-Shutter Assembly (MSA; Ferruit et al. 2022) on the NIRSpec instrument on board JWST. Two 'Tiers' of JADES data was utilized in this study: the Deep Tier NIRSpec observations are part of the GTO program ID: 1210 (PI: Lützgendorf) and in GOODS-S centred near the *Hubble* Ultra Deep Field (HUDF), obtained between 22 October and 25 October 2022 over 3 visits, and the Medium Tier observations are part of GTO program 1180 (PI: Eisenstein) obtained over a larger area in GOODS-S (see Eisenstein et al. 2023, for an overview of the field layout).

For Deep observations, the PRISM/CLEAR setup, which gives wavelength coverage in the range 0.6−5.3 µm with a spectral resolution of $R \sim 100$ (Böker et al. 2023),

and G140M/F070LP, G235M/F170LP, G395M/F290LP, and G395H/F290LP filter/grating setups were used, whereas for Medium observations all of the above but the G395H/F290LP filter/grating setup were used. For the Deep Tier, three sub-pointings were planned in the same field (although each sub-pointing had minor pointing differences), with each visit having a total of 33.613 ks of exposure in PRISM/CLEAR and 8.4 ks of exposure in each of the gratings. The Medium Tier observations were carried out in parallel to NIRCam observations, and therefore, consisted of several single pointings covering a larger sky area, with 3.8 ks of exposure time in PRISM/CLEAR and 3.1 ks of exposure time in the gratings per pointing. We note that as the sources targeted were generally high-priority targets owing to their possible high redshift nature, it was possible for one target to be covered over multiple Medium Tier pointings. We refer the readers to Bunker et al. (2023a) and Eisenstein et al. (2023) for further details about the observational setup, strategy and challenges.

The targets for spectroscopy were selected from existing deep HST-based catalogueues as well as JADES NIRCam catalogueues (Rieke et al. 2023b). Candidate high redshift galaxies with photometric redshifts $z > 5.7$, identified via the classic photometric 'drop-out' technique (e.g. Steidel et al. 1996), whereby the Lyman break in the spectrum of a galaxy is captured in adjacent broad-band filters, were assigned higher priorities. Full details of the target selection and priority classes can be found in the accompanying paper by Bunker et al. (in prep.).

The data reduction was carried out using pipelines developed by the ESA NIRSpec Science Operations Team (SOT) and the NIRSpec GTO Team (Ferruit et al. 2022, Carniani et al. in prep.). Some of the main data reduction steps implemented by the pipeline are pixel-level background subtraction, pixel-to-pixel flat-field correction, absolute flux calibration, slit-loss correction, and eventually 2-dimensional (2D) and 1-dimensional (1D) spectra extraction and co-addition. In this version of the reduction, the final 1D spectra are not extracted from the 2D spectra, but result from the weighted averaging of 1D spectra from all integrations (see Curtis-Lake et al. 2023). Due to the compact size of our LAEs, slit-loss corrections were applied by modelling it as point-like source. A nominal 3-pixel extraction aperture was used to produce the co-added 1D spectra. A detailed description of the data reduction and spectral extraction methods is given in Bunker et al. (2023a; but see also Curtis-Lake et al. 2023 and Cameron et al. 2023).

2.2. Identification of Lyman-alpha emitters

Lyα emission in the spectra of galaxies in the parent sample was identified through a combination of template fitting (Jones et al. 2024) of the R100 spectra as well as visual inspection of both the R100 and R1000 (G140M) spectra of all confirmed high-redshift galaxies in the parent sample. Using both these methods, we identified 9 candidate LAEs in Deep and 7 candidate LAEs in Medium at $z > 5.8$. We then measure the Lyα line flux by fitting a single Gaussian function to the emission in both R100 and R1000 spectra.

The Lyα line in one of the 17 LAEs at $z > 5.8$ presented in this work fell in the detector gap in R1000. With the exception of this galaxy, all visually identified LAEs encouragingly showed clear Lyα emission both in the PRISM and in G140M spectra. In Fig. 1 we show the full 1D spectrum from PRISM (R100) as well as a zoom-in on the Lyα emission identified in the G140M grating (R1000) from a selection of LAEs in our sample and the spectra of all LAEs are shown in Appendix A. In Table 1 we list the spectroscopic redshifts, the complete JADES Source name/ID and the effective exposure times in both PRISM and Gratings for the LAEs identified in this work.

Overall, we find that the line fluxes we measure from the medium resolution grating are systematically higher than the ones measured from PRISM, as can also be seen in Fig. 1, which is not surprising given the degradation in spectral resolution that PRISM spectra suffer from at shorter wavelengths. Therefore, going forward we use Lyα measurements from the G140M grating, with the exception of one source for which Lyα was in the detector gap.

2.3. Systemic redshifts

Accurate 'systemic' redshifts were measured by identifying strong emission lines in the higher resolution Grating spectra, which generally consisted of [O II], Hβ, [O III] and Hα. The redshift was derived by fitting single Gaussian functions to the strongest emission lines and using a signal to noise ratio (S/N) weighted combination of the centroids of the fits to obtain the best redshift solution. For the redshift range of our sources, the Hβ, [O III] and Hα lines fell in the G395M grating and the [O II] line fell in the G235M grating spectra. Vacuum wavelengths for all of these strong rest-frame optical lines were used for redshift determination.

We found that on average, the difference between the redshifts derived from R100 and R1000 spectra were of the order $\Delta z \sim 0.004$, but the redshifts derived from lines in the medium dispersion gratings were found to be consistent. Therefore, the redshifts that we derive and use further in the study are from the medium dispersion gratings, which also have a much narrower line-spread function (LSF) and are more sensitive to narrow emission lines. The source IDs, JADES source names, redshifts and exposure times are given in Table 1. From here on, we use the IDs to refer to the objects presented in this paper. The references for the discovery papers of these targets can be found in Bunker et al. (2023a).

2.4. UV magnitudes and slopes

UV magnitudes at rest-frame 1500 Å ($M_{\rm UV}$) were measured directly from the R100 PRISM spectra. To do this, the spectra were shifted from observed to rest-frame using the spectroscopic redshifts and a 50 Å-wide boxcar filter centred on 1500 Å to measure the median flux and error. The measured fluxes and errors were then used to calculate absolute magnitudes and errors. The distribution of the UV magnitudes and Lyα equivalent widths from our sample of LAEs is shown in Fig. 2. The UV-faint galaxies in our sample show systematically high EW(Lyα), which is likely due to the flux-limited nature of spectroscopic observations, only enabling high EW LAEs to be identified at fainter UV magnitudes.

To put our sample into perspective, we also show measurements from other LAEs at $z \gtrsim 6$ identified using JWST (Tang et al. 2023; Jung et al. 2023) or ground-based observations (Ning et al. 2023; Endsley et al. 2023) in the Figure. The LAEs presented in this work have on average fainter UV magnitudes compared to the majority of other strong LAEs at $z \gtrsim 6$ identified from ground-based telescopes in the literature. We do note, however, ground-based spectroscopic surveys around lensing clusters have been able to identify a handful of faint $z > 6$ LAEs (e.g. Hoag et al. 2019; Fuller et al. 2020; Bolan et al. 2022), which have comparable UV magnitudes to the galaxies in our sample. However, the intrinsic UV magnitudes of

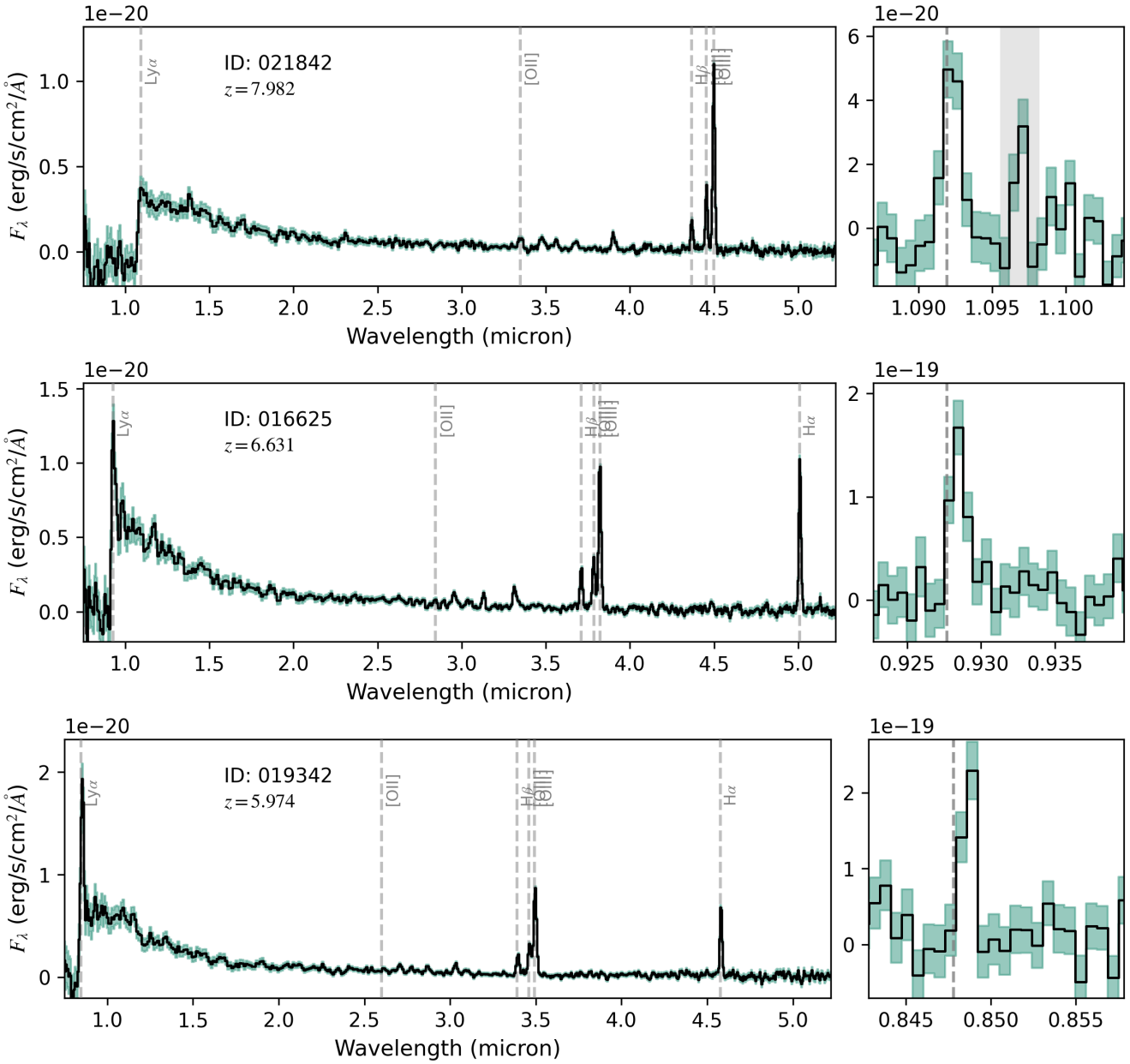

Fig. 1. Example spectra showing the PRISM (left) and G140M grating zoom-in on Lyα emission (right) of faint LAEs selected from the Deep Tier spectra in JADES, with 1σ noise shown as green shaded region. The Lyα line sensitivity in the G140M spectra is considerably higher compared to PRISM, where the decreasing spectral resolution at bluer wavelengths results in diminished emission line sensitivity. Therefore, a combination of both PRISM and Grating spectra is key to identifying Lyα emission.

lensed galaxies are prone to uncertainties from the lensing models.

We further compare our faint LAEs to those with similar UV magnitudes identified at $z < 5.7$ from the MUSE DEEP and WIDE surveys (Kerutt et al. 2022), which are also shown in Fig. 2. Interestingly, we find that the distribution of Lyα EW is highly comparable to the MUSE LAEs at a given UV magnitude. Since the MUSE LAEs shown here were selected to lie at redshifts where the IGM is not expected to significantly impact the emergent Lyα emission along the line of sight, the fact that our sample at $z \gtrsim 6$ appears to be homogeneously mixed with the MUSE sample indicates that IGM attenuation is likely not playing a very strong role on the emergent Lyα line from our galaxies. This reinforces the idea that our LAEs must be surrounded by highly ionized regions/bubbles (e.g. Witstok et al. 2024), and the shape and strength of the observed Lyα emission is likely controlled mainly by the ISM/CGM around the galaxies.

UV slopes (β, where $f_\lambda \propto \lambda^\beta$) are also measured directly from the R100 spectra by fitting a power-law function using chi-squared minimization to the flux density in the wavelength range 1340 Å–2600 Å, using the Calzetti et al. (1994) spectral windows to avoid strong emission and/or absorption features at rest-UV wavelengths. The redshifts, UV magnitudes at 1500 Å and observed UV slopes are given in Table 2.

2.5. Lyman-alpha velocity offsets

Using accurate systemic redshifts from the medium resolution grating spectra, we then use the peak of the Lyα line detected in the G140M grating spectra of our LAEs to calculate velocity

Table 1. IDs, redshifts, and exposure times for the Lyα emitting galaxies identified in this study.

ID	JADES source name	$z_{\rm spec}$	$T_{\rm exp}^{\rm PRISM}$ (ks)	$T_{\rm exp}^{\rm Grating}$ (ks)
Deep Tier				
21842	JADES-GS+53.15682−27.76716	7.982	100.0	25.0
10013682*	JADES-GS+53.16746−27.77201	7.276	66.6	16.7
4297	JADES-GS+53.15579−27.81520	6.712	33.3	8.3
16625	JADES-GS+53.16904−27.77884	6.631	100.0	25.0
18846	JADES-GS+53.13492−27.77271	6.336	100.0	25.0
19342	JADES-GS+53.16062−27.77161	5.974	100.0	25.0
9422	JADES-GS+53.12175−27.79763	5.937	100.0	25.0
6002	JADES-GS+53.11041−27.80892	5.937	100.0	25.0
19606	JADES-GS+53.17655−27.77111	5.889	33.3	8.3
10056849	JADES-GS+53.11351−27.77284	5.814	100.0	8.3
Medium Tier				
12637	JADES-GS+53.13347−27.76037	7.660	19.0	15.5
15362	JADES-GS+53.11634−27.76194	6.794	15.2	12.4
13607	JADES-GS+53.13743−27.76519	6.622	7.6	6.2
14123	JADES-GS+53.17836−27.80098	6.327	7.6	6.2
58850	JADES-GS+53.09517−27.76061	6.263	3.8	3.1
17138	JADES-GS+53.08604−27.74760	6.204	3.8	3.1
9365	JADES-GS+53.16280−27.76084	5.917	7.6	6.2

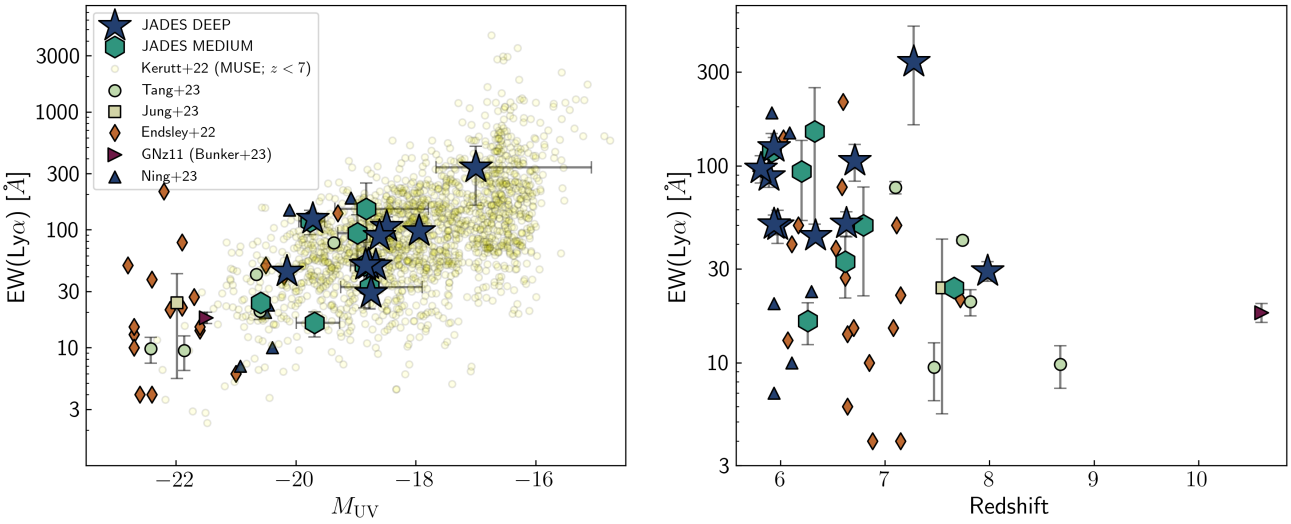

Fig. 2. Distribution of EW(Lyα) and $M_{\rm UV}$ (left) and redshift (right) of galaxies from our Deep and Medium observations. Also shown for comparison are measurements from the literature of LAEs at $z \gtrsim 6$ from Tang et al. (2023), Jung et al. (2023), Ning et al. (2023) and Endsley et al. (2023), as well as from GNz11 at $z = 10.603$ (Bunker et al. 2023b) (see Sect. 2.10 for a brief explanation about each of these data sets). In the left panel, we additionally show measurements from LAEs identified from the MUSE WIDE and DEEP surveys (Kerutt et al. 2022) at $z < 5.7$, which serve as a relevant 'reference' sample at redshifts where the IGM is not expected to impact the emergent Lyα emission significantly. We note here that several lensed LAEs also overlap with the UV magnitude distribution of our JADES sample (e.g. Hoag et al. 2019; Fuller et al. 2020; Bolan et al. 2022), which we do not show here. Our new LAE sample appears to be homogeneously mixed with the lower redshift LAE sample, indicating that the IGM may not be playing a significant role in affecting the Lyα emission reported in this paper, further stressing the presence of highly ionized regions surrounding these LAEs (see Witstok et al. 2024). The LAEs presented in this work are clearly much fainter in the UV than those that have been previously analysed in the literature at $z \gtrsim 6$. Our sample also includes the extremely high EW LAE with $M_{\rm UV} \sim -17.0$ that was recently reported by Saxena et al. (2023).

offsets from the expected Lyα emission (vacuum wavelength) at systemic redshift. As mentioned earlier, the wavelength calibrations between the different gratings were compared against the lower resolution PRISM spectra were noted to be slightly inconsistent, but the wavelengths across the grating spectra were all consistent with each other (see Bunker et al. 2023a). Therefore, inferring the observed velocity offset of Lyα from G140M spectra should not be affected by systematic offsets.

The Lyα velocity offsets were measured as follows: we implemented a Monte Carlo (MC) based approach to determine both the peak of the emission line using 100 trials, where the emission line was fitted by either a singly symmetric or

Table 2. Observed rest-frame UV magnitude ($M_{\rm UV}$) and slope (β) measured for LAEs in this study.

ID	$z_{\rm spec}$	$M_{\rm UV}$	β
Deep Tier			
21842	7.982	$-18.75^{-0.05}_{+0.05}$	-2.52 ± 0.03
10013682*	7.276	$-17.00^{-0.66}_{+1.93}$	-2.17 ± 0.60
4297	6.712	$-18.49^{-0.06}_{+0.06}$	-2.39 ± 0.09
16625	6.631	$-18.79^{-0.10}_{+0.10}$	-2.59 ± 0.02
18846	6.336	$-20.15^{-0.05}_{+0.05}$	-2.43 ± 0.01
19342	5.974	$-18.67^{-0.03}_{+0.03}$	-2.75 ± 0.04
9422	5.937	$-19.72^{-0.04}_{+0.04}$	-2.33 ± 0.04
6002	5.937	$-18.84^{-0.07}_{+0.07}$	-2.59 ± 0.01
19606	5.889	$-18.61^{-0.17}_{+0.15}$	-2.70 ± 0.06
10056849	5.814	$-17.95^{-0.07}_{+0.06}$	-2.49 ± 0.04
Medium Tier			
12637	7.660	$-20.59^{-0.07}_{+0.07}$	-2.20 ± 0.02
15362	6.794	$-18.86^{-0.23}_{+0.29}$	-2.14 ± 0.15
13607	6.622	$-18.77^{-0.88}_{+0.48}$	-1.79 ± 0.29
14123	6.327	$-18.83^{-1.04}_{+0.52}$	-2.26 ± 0.21
58850	6.263	$-19.96^{-0.42}_{+0.30}$	-1.93 ± 0.06
17138	6.204	$-18.97^{-0.47}_{+0.33}$	-2.26 ± 0.54
9365	5.917	$-19.76^{-0.24}_{+0.19}$	-2.52 ± 0.09

asymmetric Gaussian, depending on whichever function yielded a lower chi-squared statistic and hence, a better fit to the data. The spectral resolution of our $R \sim 1000$ spectra is unfortunately not high enough to properly characterize the line shape, therefore we do not enforce a symmetric or asymmetric Gaussian fit, but simply pick the model that returns a better fit.

For each MC trial, we perturbed the line fluxes by randomly sampling from the error spectrum. The line fitting was performed for each trial, with the median of the Gaussian centre then used to measure the velocity offset, and one sigma dispersion on the line centre distribution used to derive the error on this measurement. Due to the nature of this method, emission lines with high S/N naturally have lower errors on the velocity offsets.

2.6. Other emission line measurements

The rest-frame optical emission line fluxes for all LAEs are measured from the higher spectral resolution grating spectra, unless the lines are not clearly detected in the grating. In that case we measure and report the line fluxes from the PRISM spectra. The main emission lines that we measure for our sample of LAEs are [O II] $\lambda\lambda$3726, 3729 (which appear to be blended), Hβ, [O III] $\lambda\lambda$4959, 5007 and Hα.

We once again fit single Gaussian functions to all of these lines, measuring the local continuum from a wavelength region adjacent to the emission line. Using these line fluxes we also calculate line ratios such as [O III] λ5007/[O II] $\lambda\lambda$3726, 3729 (O32) and ([O II] $\lambda\lambda$3726, 3729 + [O III] $\lambda\lambda$4959, 5007)/Hβ (R23).

2.7. Dust measurements from Balmer decrements

Here we use the Balmer emission line decrements calculated from Hα/Hβ (or Hβ/Hγ when Hα is not within the spectral coverage). We calculate the intrinsic ratio of these lines using PYNEB (Luridiana et al. 2015), assuming a temperature of 10^4 K and electron density of 100 cm^{-3}. This gives an intrinsic Hα/Hβ ratio of 2.863. We assume the dust attenuation curve for the Small Magellanic Cloud (SMC; Gordon et al. 2003), which has been shown to be the most appropriate for high redshift galaxies (e.g. Shivaei et al. 2020).

Dust attenuation, $E(B-V)$ is then calculated by comparing the observed Balmer line ratios with the intrinsic. We note that the Hα line is detected for all but one galaxy in our sample, and therefore, we primarily use the observed Hα/Hβ ratios to calculate dust attenuation across our sample, but for $z > 7$ LAEs, where Hα moves out of NIRSpec coverage, we use Hβ/Hγ.

2.8. Ionizing photon production efficiency

We use the Hα flux (or Hβ when Hα is not within the spectral coverage, using an intrinsic ratio of 2.863 under the assumptions that were mentioned in the previous section) and the monochromatic luminosity at 1500 Å to calculate the ionizing photon production efficiency, or $\xi_{\rm ion}$, given by

$$\left(\frac{\xi_{\rm ion}}{\rm erg^{-1}\ Hz}\right) = \frac{N(\rm H^0)}{L_{1500,int}} \quad (1)$$

where $N(\rm H^0)$ is the intrinsic hydrogen ionizing photon production rate in units of s^{-1} and $L_{1500,\rm int}$ is the intrinsic (dust-corrected) luminosity density at rest-frame 1500 Å in units of erg s^{-1} Hz^{-1}.

The Hα line (or other Balmer lines) luminosity can be used to calculate the intrinsic ionizing photon production rate. Assuming the same physical conditions as before of $T_{\rm e} = 10^4$ K and $n_{\rm e} = 100$ cm^{-3},

$$N(\rm H^0) \times (1 - f_{esc}) = 7.3 \times 10^{11} L(H\alpha) \quad (2)$$

where $f_{\rm esc}$ is the escape fraction of LyC photons out of the galaxy (e.g. Maseda et al. 2020; Simmonds et al. 2023). To calculate $\xi_{\rm ion}$ for our LAEs, we assume Case-B recombination, that is $f_{\rm esc}(\rm LyC) = 0$ (see Sect. 5, however, for a discussion about non-zero $f_{\rm esc}(\rm LyC)$).

2.9. Lyman-alpha escape fractions

We now use the strength of Balmer emission lines seen in the spectrum together with the inferred dust attenuation to derive a Lyα escape fraction for all LAEs in our sample. Assuming Case-B recombination, $n_{\rm e} = 100$ cm^{-3} and $T_{\rm e} = 10\,000$ K, the intrinsic Lyα/Hα ratio is 8.2 (e.g. Osterbrock 1989). We then calculate $f_{\rm esc}$(Lyα) as the ratio of the observed (dust-corrected) Lyα to Balmer line emission to the intrinsic ratio, which for the Hα emission line looks like: $f_{\rm esc}(\rm Ly\alpha) = L(\rm Ly\alpha)/(8.2 \times L(H\alpha))$.

The observed Lyα properties, which include line fluxes, equivalent widths, velocity offset from systemic redshift and the Lyα escape fraction ($f_{\rm esc}$) are given in Table 3.

2.10. Comparison samples from the literature

To put our results into a more global context while also increasing the baseline of several physical parameters that were also measured from our sample of faint LAEs, we describe here a selection of literature samples of LAEs at $z \gtrsim 6$ with which

Table 3. Observed Lyα emission properties of LAEs in this study.

ID	$z_{\rm spec}$	$F^{\rm Ly\alpha}_{\rm R100}$ ($\times10^{-18}$ cgs)	$\rm EW^{Ly\alpha}_{R100}$ (Å)	$F^{\rm Ly\alpha}_{\rm R1000}$ ($\times10^{-18}$ cgs)	$\rm EW^{Ly\alpha}_{R1000}$ (Å)	$\Delta v^{\rm Ly\alpha}_{\rm sys}$ (km s^{-1})	$f_{\rm esc}$(Lyα)
Deep Tier							
21842	7.982	0.3 ± 0.2	14.1 ± 5.7	0.7 ± 0.1	29.2 ± 3.3	166.5 ± 30.5	0.09 ± 0.01
10013682*	7.276	1.5 ± 0.2	258.5 ± 43.0	2.2 ± 0.5	337.2 ± 175.5	178.4 ± 21.1	0.93 ± 0.12
4297	6.712	0.9 ± 0.3	35.3 ± 10.5	2.7 ± 0.3	106.2 ± 22.5	153.0 ± 76.1	0.55 ± 0.04
16625	6.631	13.7 ± 2.0	32.0 ± 4.8	21.8 ± 4.8	51.0 ± 7.4	244.2 ± 25.8	0.14 ± 0.02
18846	6.336	4.2 ± 2.1	24.1 ± 0.9	7.7 ± 1.3	44.5 ± 1.7	139.4 ± 5.1	0.31 ± 0.01
19342	5.974	2.4 ± 0.2	55.1 ± 6.3	2.2 ± 0.5	49.9 ± 9.6	257.0 ± 21.2	0.24 ± 0.04
9422	5.937	9.3 ± 2.7	109.2 ± 14.7	10.6 ± 0.9	124.4 ± 17.2	147.6 ± 15.1	0.26 ± 0.01
6002	5.937	2.0 ± 0.2	35.3 ± 2.8	2.9 ± 0.6	50.5 ± 5.8	181.0 ± 42.1	0.43 ± 0.04
19606	5.889	6.3 ± 0.4	111.2 ± 26.3	–	–	–	0.50 ± 0.03
10056849	5.814	4.9 ± 0.3	127.0 ± 10.5	3.8 ± 0.5	97.2 ± 15.2	233.0 ± 36.3	0.42 ± 0.06
Medium Tier							
12637	7.660	0.6 ± 0.2	3.5 ± 0.9	4.2 ± 0.3	24.0 ± 1.9	277.2 ± 34.4	0.13 ± 0.01
15362	6.794	–	–	1.5 ± 0.7	50.0 ± 28.2	27.0 ± 124.6	0.20 ± 0.07
13607	6.622	0.2 ± 0.2	2.9 ± 2.1	2.4 ± 0.9	29.4 ± 9.0	116.8 ± 61.1	0.26 ± 0.08
14123	6.327	7.0 ± 2.0	241.2 ± 160.8	4.3 ± 1.2	150.1 ± 99.6	194.2 ± 43.4	0.35 ± 0.07
58850	6.263	9.1 ± 0.8	4.8 ± 2.9	3.1 ± 0.8	16.3 ± 3.9	254.6 ± 43.1	0.06 ± 0.01
17138	6.204	3.0 ± 1.1	65.0 ± 22.8	4.6 ± 2.1	93.6 ± 40.9	0.0 ± 71.9	0.40 ± 0.10
9365	5.917	12.2 ± 1.4	109.5 ± 16.6	11.2 ± 1.9	118.4 ± 27.6	256.7 ± 60.9	0.28 ± 0.04

Notes. The flux units are erg s^{-1} cm^{-2} (cgs).

we compare our results. Perhaps the most immediate comparison is offered by LAEs identified by Tang et al. (2023) using JWST spectroscopy through the CEERS survey (see also Fujimoto et al. 2023). We also include CEERS results from Jung et al. (2023) in this study. Since CEERS is shallower and wider than JADES, it more efficiently selects the rarer UV-bright galaxies by probing a much larger volume at high redshifts.

We also use the compilation of $z \gtrsim 6$ LAEs from Endsley et al. (2022) that have ALMA emission line measurements, enabling robust measurements of the Lyα velocity offsets. This compilation includes LAEs from the ALMA REBELS survey (Bouwens et al. 2022) as well as other LAEs at $z > 6$: CLM1 (Cuby et al. 2003; Willott et al. 2015), WMH5 (Willott et al. 2015), B14-65666 (Furusawa et al. 2016; Hashimoto et al. 2019), EGS-zs8-1 (Oesch et al. 2015; Stark et al. 2017), COS-z7-1 (Pentericci et al. 2016; Laporte et al. 2017; Stark et al. 2017), COSMOS24108 (Pentericci et al. 2016, 2018b), NTTDF6345 (Pentericci et al. 2011, 2016), UDS16291 (Pentericci et al. 2016, 2018b), BDF-3299 (Vanzella et al. 2011; Maiolino et al. 2015; Carniani et al. 2017), RXJ2248-ID3 (Mainali et al. 2017), A383-5.2 (Stark et al. 2015; Knudsen et al. 2016), VR7 (Matthee et al. 2019, 2020), CR7 (Sobral et al. 2015; Matthee et al. 2017b) and Himiko (Ouchi et al. 2013; Carniani et al. 2018).

We also include Lyα and Hα based measurements from Ning et al. (2023) as well as Simmonds et al. (2023), which use narrow/medium band photometry to infer Hα strengths in spectroscopically confirmed LAEs at $z \sim 6$ identified from MUSE data, enabling the determination of $f_{\rm esc}$(Lyα) and $\xi_{\rm ion}$.

Finally, we also use the Lyα emission measurements from GNz-11, spectroscopically confirmed to lie at $z = 10.60$ with weak Lyα emission detected in the medium band NIRSpec gratings (Bunker et al. 2023b).

3. Spectroscopic properties of Lyman-alpha emitters at $z \gtrsim 5.8$

In this section we explore the general spectroscopic properties of LAEs identified in the JADES Deep and Medium Tier surveys, with the aim of comparing the ionization and chemical enrichment of LAEs with the general galaxy population at $z \gtrsim 6$ as well as evaluating the ionizing photon production efficiencies of LAEs across cosmic time.

3.1. Chemical enrichment and dust

In Fig. 3, we show R23 vs. O32 line ratios for our Deep- and Medium-Tier samples of LAEs. These line ratios are widely used tracers of metallicity and ionization parameter respectively, with the former forming a two-valued relation with metallicity. For comparison, we show $z < 0.1$ galaxies from the SDSS MPA-JHU catalogues (Aihara et al. 2011)[1], as well as non-Lyman-alpha-emitting galaxies at $z > 5.5$ from JADES Deep (Cameron et al. 2023), and measurements from individual and stacked galaxies at $z \gtrsim 5$ not selected on presence or otherwise of Lyα (Mascia et al. 2023; Nakajima et al. 2023; Sanders et al. 2023; Tang et al. 2023). Our LAEs on average appear to be metal poor with high ionization parameters, lying away from the locus of typical star-forming galaxies at $z < 0.1$ from SDSS towards high O32 and R23. Instead, they are more similar to what has been reported for the general galaxy population at $z > 6$.

We do note that LAEs from our Deep Tier survey, which tend to have fainter UV magnitudes ($\lesssim$−20.1), show slightly higher O32 ratios and lower R23 ratios compared to LAEs found in the Medium Tier survey as well as other brighter LAEs at $z > 6$. This is consistent with the finding in Cameron et al. (2023) that $z \sim 6$ galaxies from deep JADES observations show much higher

[1] https://www.sdss3.org/dr10/spectro/galaxy_mpajhu.php

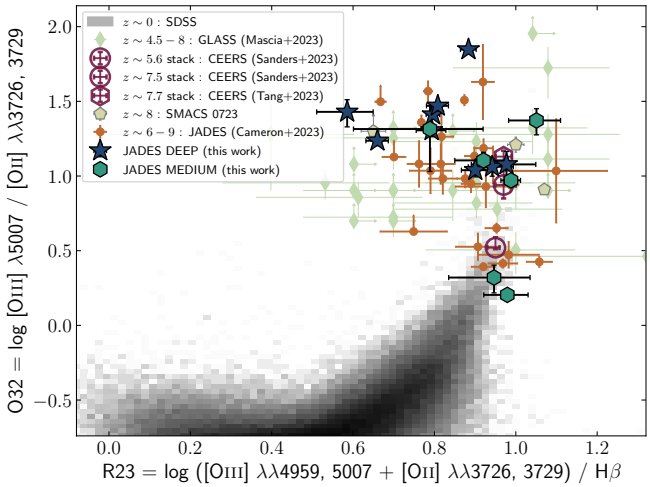

Fig. 3. Comparison of R23 and O32 ratios of LAEs with the general galaxy populations inferred from NIRSpec observations at $z \gtrsim 6$. Orange circles show JADES Deep galaxies from Cameron et al. (2023) which are not LAEs. Diamonds and pentagons show measurements from individual lensed galaxies at $z \gtrsim 5$ (Mascia et al. 2023; Nakajima et al. 2023). Measurements from stacked galaxies at $z \sim 5.6$–7.7 are shown as hollow purple markers (Sanders et al. 2023; Tang et al. 2023). Also shown are measurements from SDSS for $z < 0.1$ star-forming galaxies (Aihara et al. 2011). Overall, we find that our faint LAEs occupy a similar parameter to that occupied by the general star-forming galaxy population at $z \gtrsim 6$. This also highlights that the observed presence of Lyα emission in reionization era galaxies is driven by external factors, and not necessarily by the ISM/stellar properties of the galaxies. Interestingly, UV-faint LAEs from our sample tend to show higher O32 and lower R23 ratios than the UV-bright ones.

O32, and lower R23 than those measured from stacks of CEERS galaxies (Sanders et al. 2023), which are typically brighter. This is indicative of higher ionization parameters and lower chemical enrichment in fainter, less massive galaxies at $z > 6$.

Overall we find that the parameter space on this plot occupied by LAEs at $z \gtrsim 6$ is roughly the same as the general galaxy population at these redshifts. This suggests that the detection of Lyα emission from a galaxy in the EoR may not necessarily depend on the chemical or ionization state that is in, but may be more driven by opportune sight-lines probing sufficiently ionized regions of the Universe.

We do not measure any presence of dust from Balmer decrements derived from Hα/Hβ ratios for our LAEs (in agreement with Sandles et al. 2023), which suggests that such systems are relatively dust-free, which is also a prerequisite for the leakage of significant fractions of Lyman continuum photons from a galaxy into the IGM.

3.2. Ionizing photon production

The average ionizing photon production efficiency across our sample of faint LAEs is $\xi_{\rm ion} = 25.57\,{\rm Hz\,erg^{-1}}$ shown as a dashed line in Fig. 4, which is 0.3–0.4 dex higher than the canonical value of 25.2–25.3 typically assumed in reionization models (e.g. Kuhlen & Faucher-Giguère 2012; Robertson et al. 2013). The higher $\xi_{\rm ion}$ values may also be indicative of elevated ionizing photon production due to non-thermal processes such as X-ray binary stars, whose impact is expected to increase with decreasing metallicities (e.g. Saxena et al. 2021).

When comparing with other measurements for LAEs at the highest redshifts in the literature, we do not see significant evolution in $\xi_{\rm ion}$ as a function of redshift at $z > 6$. Our measurements are higher than $\xi_{\rm ion} = 25.33\,{\rm Hz\,erg^{-1}}$ that was reported for a sample of UV faint galaxies in the redshift range $3 < z < 7$ by Prieto-Lyon et al. (2023b), where they reported a ∼0.1 dex higher measurement for LAEs.

Interestingly, there does not seem to be any strong dependence of $\xi_{\rm ion}$ on the equivalent width of Lyα emission either. Assuming Case B recombination and $f_{\rm esc}$(Lyα) of unity, $\xi_{\rm ion}$ may be expected to increase linearly with EW(Lyα). The fact that there is no clear correlation between these two quantities across a wider sample of known LAEs at $z > 6$ spanning orders of magnitude in brightness suggests that the mechanisms that are responsible for the production of ionizing photons in a galaxy are not the ones that also control the escape of Lyα photons from the galaxy. In other words, the neutral gas and dust content, which preferentially affects the transmission of Lyα photons, does not seem to closely depend on properties such as stellar metallicities or ages that control the production of ionizing photons.

Combined with the lack of redshift evolution in $\xi_{\rm ion}$, the picture that emerges is that the ionizing photon production is not closely linked to the strength of the emergent Lyα line emission, as it is likely more dependent on the physical and chemical properties of star-forming regions that do not seem to evolve strongly between $z = 6$–8.5. This may have important consequences for modelling the production and escape of ionizing photons from galaxies within the reionization epoch, which we revisit in Sect. 5. The chemical enrichment and ionizing properties of LAEs in this study are given in Table 4.

4. The escape of Lyman-alpha photons

In this section we explore which galaxy property best traces the Lyα velocity offset from the systemic redshift as well as the escape fraction of Lyα photons, $f_{\rm esc}$(Lyα), which are widely regarded to be tracing escape channels for hydrogen ionizing LyC photons. The goal of this section is to determine the best tracer for LyC leakage when Lyα emission may not be visible from galaxies in the reionization era.

4.1. High Lyman-alpha escape fraction implies more Lyman-alpha photons escape closer to systemic velocity

We begin by demonstrating that the escape fraction of Lyα photons appears to be anti-correlated with the velocity offset of the Lyα emission compared to the systemic redshift of a galaxy, as shown in Fig. 5. The anti-correlation is not as strong when considering only our magnitude limited JADES sample (p-value = 0.39), but when expanding the dynamic range by including other known strong LAEs at $z > 6$ with Lyα velocity offset and escape fraction measurements, we recover an anti-correlation with a very high significance (p-value = 8.7×10^{-5}).

This anti-correlation can be explained using neutral gas column densities – a low column density of neutral gas will lead to less resonant scattering of Lyα photons out of the line of sight, thereby resulting in both a high observed $f_{\rm esc}$(Lyα) as well as low velocity offsets from systemic as has been predicted by theoretical models (Neufeld 1990; Dijkstra et al. 2006; Verhamme et al. 2006; Laursen et al. 2009). Low neutral gas density environments are also though to be conducive to the escape of LyC photons from a galaxy (at least along the same line of sight as Lyα). Therefore, both Lyα velocity offsets and/or escape fractions can

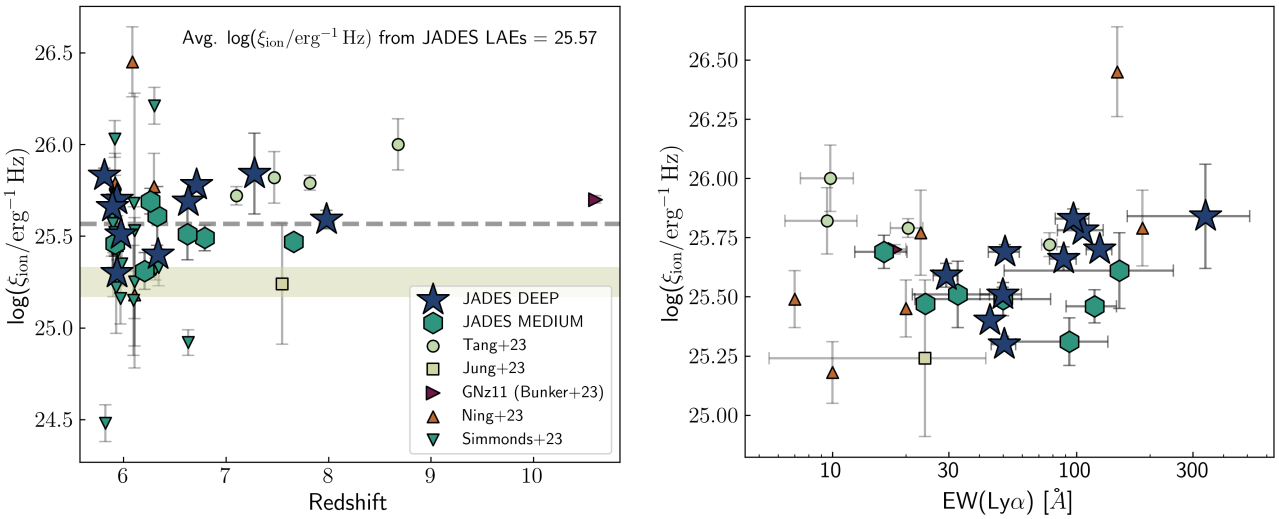

Fig. 4. Dependence of the ionizing photon production efficiency ($\xi_{\rm ion}$) from LAEs at $z \gtrsim 6$ on redshift (left) and EW(Lyα) (right). The dashed line indicates the average $\xi_{\rm ion}$ value (log($\xi_{\rm ion}$/erg^{-1} Hz) = 25.57) measured across the new LAEs reported in this study. The shaded region marks the canonical value of log($\xi_{\rm ion}$/erg^{-1} Hz) = 25.2–25.3 from Kuhlen & Faucher-Giguère (2012), Robertson et al. (2013, 2015). Overall, we do not find a significant evolution in the $\xi_{\rm ion}$ of LAEs across redshifts particularly at $z > 6$, indicating that the ionizing properties do not seem to evolve strongly between $z = 6$–8.5. There is also no strong correlation between $\xi_{\rm ion}$ and the strength of Lyα emission across LAEs at $z > 6$, which one would naively expect from simple Case B recombination in the absence of significant absorption/scattering of Lyα photons. This lack of correlation indicates that the processes that control the escape of Lyα photons may not necessarily be dependent on the processes that produce ionizing photons.

be important to ascertain the escape of ionizing photons from galaxies that drive reionization.

In the following sections we explore correlations between various galaxy properties and each of Lyα velocity offset and $f_{\rm esc}$(Lyα) to establish dependencies and/or observational biases that impact the Lyα strength and line profile in LAEs at $z \gtrsim 6$.

4.2. Insights from Lyman-alpha velocity offsets

In Fig. 6 we compare the Lyα velocity offsets observed for our sample of galaxies with other observables that trace both the underlying stellar populations as well as the state of the ISM. We also include measurements of brighter LAEs in the EoR from the literature to increase the baseline of any trends that may become apparent.

When comparing Lyα velocity offsets with EW(Lyα), we find that our JADES sample shows a very weak anti-correlation (p-value = 0.59), whereas the extended $z > 6$ sample shows a strong anti-correlation (p-value = 4.3×10^{-4}), albeit with considerable scatter, as shown in Fig. 6 (top left). Such an anti-correlation has previously been reported in the literature across redshifts (e.g. Izotov et al. 2021) and mainly stems from the resonant scattering of Lyα photons by the neutral gas within the galaxies – a higher velocity offset compared to the systemic redshift is indicative of more resonant scattering of the emergent Lyα photons, which results in decreased Lyα flux observed along the line-of-sight. Therefore, the same scattering mechanism is responsible for increased offset from systemic velocity as well as the reduction of EW(Lyα) across galaxies. With high EW Lyα emission that peaks close to the systemic redshift likely tracing low covering fractions of neutral gas, galaxies that exhibit such Lyα profiles and strengths are also likely to be leaking significant amounts of LyC photons (Verhamme et al. 2015, 2017).

For the sample of UV-faint LAEs probed by the JADES sample presented in this paper, we find the equivalent widths to be higher and the velocity offsets to be lower compared to UV-bright LAEs in the literature (Fig. 6, top right), which may indicate that UV-fainter LAEs could be more likely to host conditions required for efficient Lyα as well as LyC escape (see also Prieto-Lyon et al. 2023a), which we subsequently explore in detail in the later sections. For our JADES sample, do not find any correlation between the Lyα velocity offset and the UV magnitude (p-value = 0.96). However, when looking at the extended LAE sample with a larger dynamic range in UV magnitude, we find that the Lyα velocity offsets appear to be reducing at fainter UV magnitudes (p-value = 0.001). There have been suggestions in the literature that the Lyα velocity offset increases with stellar mass (e.g. Erb et al. 2014; Hayes et al. 2023), which may explain the trends that we see with UV magnitude for the full sample.

Particularly within the context of ionized bubbles within which LAEs in the EoR must reside to be able to freely transmit Lyα photons along the line of sight, smaller velocity offsets are also expected to trace large ionized bubble sizes (see Mason & Gronke 2020; Saxena et al. 2023, for example), which would lead to considerably less attenuation by the intervening IGM and therefore, higher transmission of Lyα leading to high equivalent width measurements.

Next we compare the Lyα offset with spectroscopic indicators of the ionization parameter (that is the ratio of ionizing photons to the hydrogen density) probed by indicators such as the O32 ratio (Fig. 6, bottom left). Interestingly, we observe a mild positive correlation between O32 and Lyα velocity offset, but there is considerable scatter on this relation and the relation becomes less significant when we also include LAEs from Tang et al. (2023). A high O32 ratio has been proposed as an indicator for both high Lyα and LyC escape (e.g. Izotov et al. 2021) and we do find that our UV-faint LAEs with small velocity offsets on average show high O32 ratios. However, given a lack of strong correlation between O32 and Lyα velocity offset we conclude that high O32 ratios are a

Table 4. Chemical enrichment, ionization properties, and Lyman continuum escape fractions of Lyα emitters presented in this study.

ID	z_{spec}	$F^{H\beta}$ ($\times 10^{-19}$ cgs)	$F^{H\alpha}$ ($\times 10^{-19}$ cgs)	$\log(\xi_{ion}/Hz\,erg^{-1})$	[O III]/[O II] (O32)	([O II]+[O III])/Hβ (R23)	f_{esc}(LyC)
Deep Tier							
21842	7.982	3.2 ± 0.5	–	$25.59^{+0.05}_{-0.05}$	11.5 ± 1.6	8.8 ± 1.1	0.08 ± 0.01
10013682	7.276	0.8 ± 0.2	–	$25.66^{+0.11}_{-0.14}$	12.0 ± 2.6	9.5 ± 1.7	0.03 ± 0.01
4297	6.712	5.3 ± 0.6	16.2 ± 0.04	$25.78^{+0.02}_{-0.02}$	19.8 ± 4.7	7.5 ± 1.4	0.02 ± 0.01
16625	6.631	5.9 ± 0.3	16.5 ± 0.2	$25.69^{+0.03}_{-0.04}$	24.5 ± 3.0	4.9 ± 0.5	0.04 ± 0.01
18846	6.336	11.4 ± 0.2	30.3 ± 0.3	$25.32^{+0.01}_{-0.01}$	25.8 ± 1.3	6.3 ± 0.2	0.07 ± 0.01
19342	5.974	4.1 ± 0.2	10.8 ± 0.3	$25.42^{+0.01}_{-0.01}$	29.5 ± 1.8	6.4 ± 0.4	0.06 ± 0.01
9422	5.937	18.4 ± 0.1	50.0 ± 0.7	$25.65^{+0.01}_{-0.01}$	70.6 ± 4.1	7.7 ± 0.3	0.01 ± 0.001
6002	5.937	2.8 ± 0.1	8.1 ± 0.2	$25.19^{+0.02}_{-0.02}$	10.9 ± 1.1	7.6 ± 0.6	0.06 ± 0.01
19606	5.889	4.6 ± 0.4	13.5 ± 0.5	$25.51^{+0.04}_{-0.05}$	21.9 ± 2.5	7.5 ± 0.7	0.06 ± 0.01
10056849	5.814	4.0 ± 0.4	10.9 ± 0.3	$25.65^{+0.02}_{-0.02}$	17.22 ± 1.3	4.6 ± 0.3	0.03 ± 0.01
Medium Tier							
12637	7.660	13.9 ± 0.5	–	$25.45^{+0.02}_{-0.02}$	9.4 ± 0.6	9.7 ± 0.5	0.10 ± 0.01
15362	6.794	4.3 ± 0.4	11.8 ± 1.2	$25.49^{+0.07}_{-0.09}$	2.7 ± 0.3	6.2 ± 0.6	0.16 ± 0.02
13607	6.622	3.6 ± 0.5	11.9 ± 0.9	$25.51^{+0.14}_{-0.22}$	1.6 ± 0.1	11.5 ± 1.1	0.80 ± 0.11
14123	6.327	5.6 ± 0.9	15.1 ± 1.2	$25.61^{+0.16}_{-0.25}$	12.2 ± 2.6	8.9 ± 2.4	0.04 ± 0.01
58850	6.263	26.0 ± 1.7	65.9 ± 2.0	$25.83^{+0.09}_{-0.11}$	23.6 ± 4.7	11.2 ± 1.6	0.02 ± 0.01
17138	6.204	3.6 ± 3.0 (†)	10.4 ± 1.9	$25.31^{+0.10}_{-0.13}$	1.8 ± 0.3	8.1 ± 1.2	0.38 ± 0.10
9365	5.917	11.1 ± 1.8	30.8 ± 1.3	$25.40^{+0.07}_{-0.08}$	12.3 ± 1.7	10.1 ± 1.2	0.14 ± 0.02

Notes. The flux units are erg s^{-1} cm^{-2} (cgs). (†)The Hβ line was affected by a possible cosmic ray in the spectrum, and therefore, Hα flux was used to estimate Hβ flux assuming no dust.

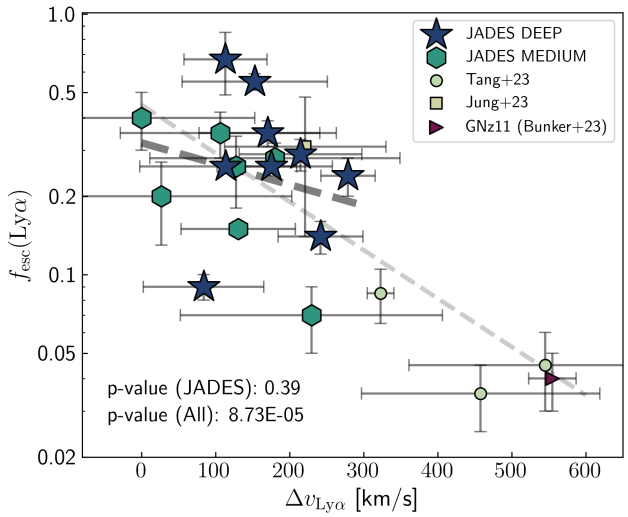

Fig. 5. Lyα velocity offset vs. f_{esc}(Lyα), where a strong anti-correlation between these quantities is observed both in the JADES-only sample (thick dashed line) as well as when looking at the full high redshift Lyα emitter sample (thin dashed line). High f_{esc}(Lyα) and small velocity offsets likely trace relatively dust and gas-free conditions, which neither leads to considerable resonant scattering of Lyα photons as they travel along a sight line, nor does it attenuate Lyα emission via absorption and scattering.

necessary but not a sufficient condition for efficient ionizing photon escape (see also Choustikov et al. 2024).

Looking at the dependence of Lyα velocity offset on EW(Hβ), which is a good tracer for star formation rates and consequently the production rates of Hydrogen ionizing photons, only for our JADES sample, we do not find any strong correlation (Fig. 6, bottom right). EW(Hβ) has also been proposed as a robust indicator of f_{esc}(LyC) (e.g. Zackrisson et al. 2013; Flury et al. 2022b). The requirement of a relatively high EW(Hβ) is perhaps similar in nature to the requirement of high O32 from LyC leaking galaxies, necessary but insufficient on its own to enable efficient Lyα/LyC escape.

4.3. Insights from the Lyman-alpha escape fraction

We now explore the dependence of f_{esc}(Lyα) measured directly from the spectra with other galaxy properties and show the dependence of f_{esc}(Lyα) on EW(Lyα), M_{UV}, O32 and EW(Hβ) in Fig. 7.

We find a strong correlation at high significance levels between f_{esc}(Lyα) and EW(Lyα) for both our JADES LAEs (p-value $= 4.6 \times 10^{-5}$) as well as the extended sample (p-value $= 3.1 \times 10^{-7}$) (Fig. 7, top left) Since f_{esc}(Lyα) is calculated using the observed ratio of Lyα to Hα (or Hβ) emission, this strong correlation suggests that the Hα (or Hβ) line fluxes do not scale in proportion with the Lyα escape fractions in LAEs with higher EW Lyα emission.

We also find that the observed f_{esc}(Lyα) (just like EW(Lyα)) increases consistently with decreasing UV magnitudes (Fig. 7, top right), with strong correlations seen both for the JADES sample (p-value $= 4.3 \times 10^{-2}$) and the full sample (p-value $= 1.3 \times 10^{-2}$). This may be indicative of decreasing neutral gas covering fractions that potentially play a more important role in dictating the strength of the observed Lyα emission than the intrinsic production of ionizing photons.

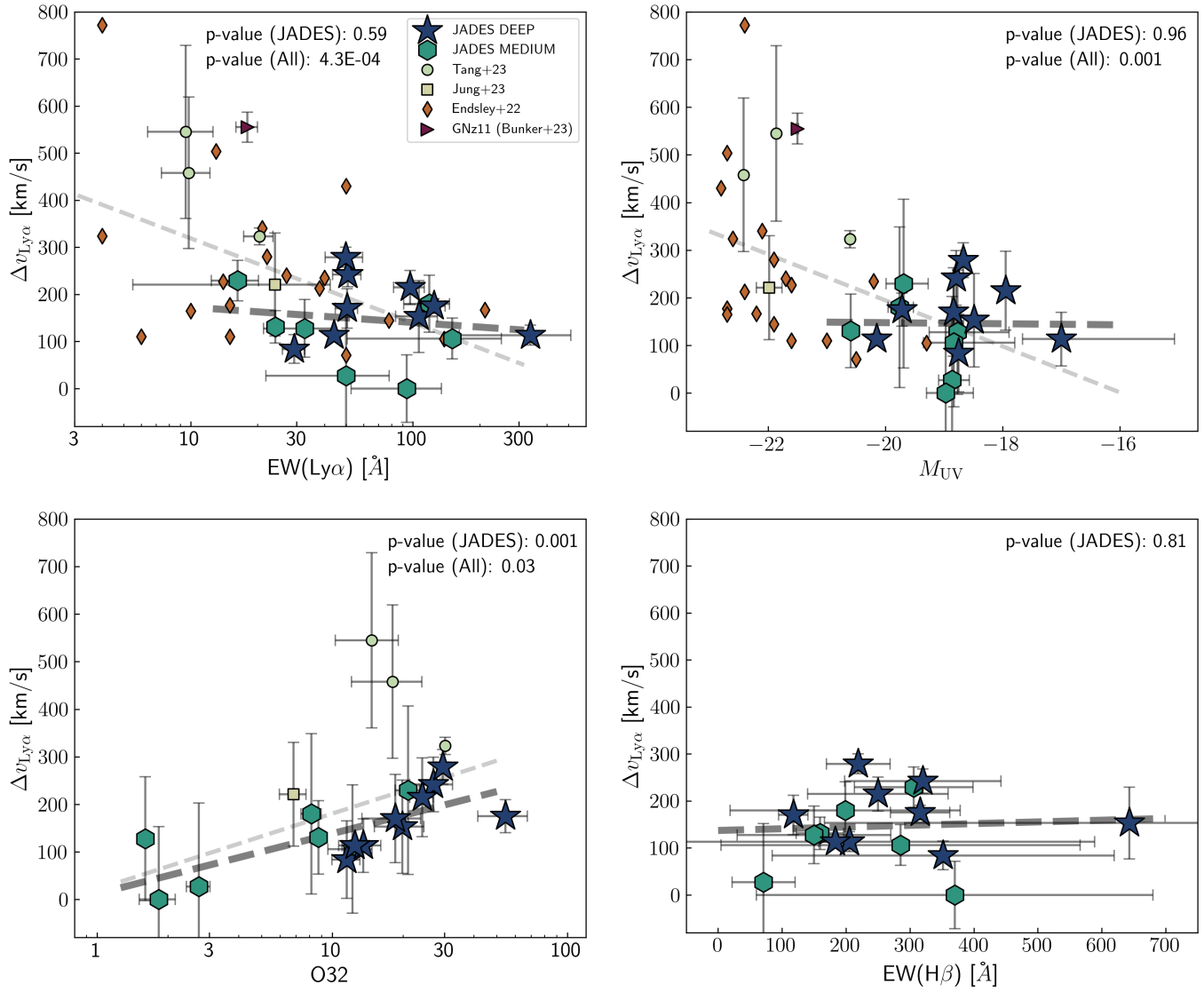

Fig. 6. Dependence of the Lyα velocity offset on EW(Lyα) (top left), M_{UV} (top right), [O III]/[O II] ratio (O32) (bottom left) and EW(Hβ) (bottom right). In these plots, we show the correlations between quantities derived using only our JADES sample as the thicker, darker dashed line, and those derived using the extended LAE sample with the thinner, lighter dashed line, with p-values given for both. We find an anti-correlation between Lyα velocity offset and EW(Lyα), which is likely driven by the neutral gas content in the galaxy, whereby a larger reservoir of neutral gas both attenuates Lyα flux close to the systemic velocity as well as moves the apparent peak of the emission line away from systemic velocity due to resonant scattering of Lyα photons. Lyα emission from UV-fainter LAEs also peaks closer to the systemic redshift, which is indicative of decreasing neutral gas content at fainter luminosities/galaxy masses. No strong correlations exist between Lyα offset and O32 ratios or EW(Hβ), interestingly with three low Lyα velocity offset sources showing low (<3) O32 ratios.

However, We note that the lack of low f_{esc}(Lyα) (or low EW(Lyα)) detections from the faintest galaxies may also be a consequence of the flux limited nature of the spectroscopic data used in this study. It is also worth noting that the lack of high f_{esc}(Lyα) observations from the UV-brightest galaxies is once again indicative of increasing neutral gas fractions in more luminous/massive systems, which likely attenuates and/or scatters the Lyα flux along the line-of-sight.

Comparing with O32 and EW(Hβ), we find that neither of these quantities correlates strongly with f_{esc}(Lyα) across both the JADES-only sample as well as when including other LAEs (p-values > 0.4). Several studies at lower redshifts have found that O32 correlates with f_{esc}(Lyα) (e.g. Yang et al. 2017; Flury et al. 2022b), whereas Izotov et al. (2020) reported no correlation between O32 and f_{esc}(Lyα) for their sample of extreme [O III] emitters at low redshifts. We note that high O32 ratios and/or EW(Hβ) are perhaps needed to have a higher chance of observing high f_{esc}(Lyα) as was also noted by Flury et al. (2022b), but there is considerable scatter in the O32 ratios that we measure for our LAEs, with some LAEs showing O32 < 3. Therefore, the O32 ratio may not be a good predictor of the expected f_{esc}(Lyα) (and consequently LyC) from galaxies in the reionization era.

4.4. Role of the IGM in attenuating Lyman-alpha emission at $z > 6$

Finally in this section, we look at the evolution of f_{esc}(Lyα) with redshift, focusing particularly on $z \gtrsim 6$ where the IGM is expected to play a dominant role in attenuating Lyα emission, unless the LAEs live in large ionized bubbles. In Fig. 8 we

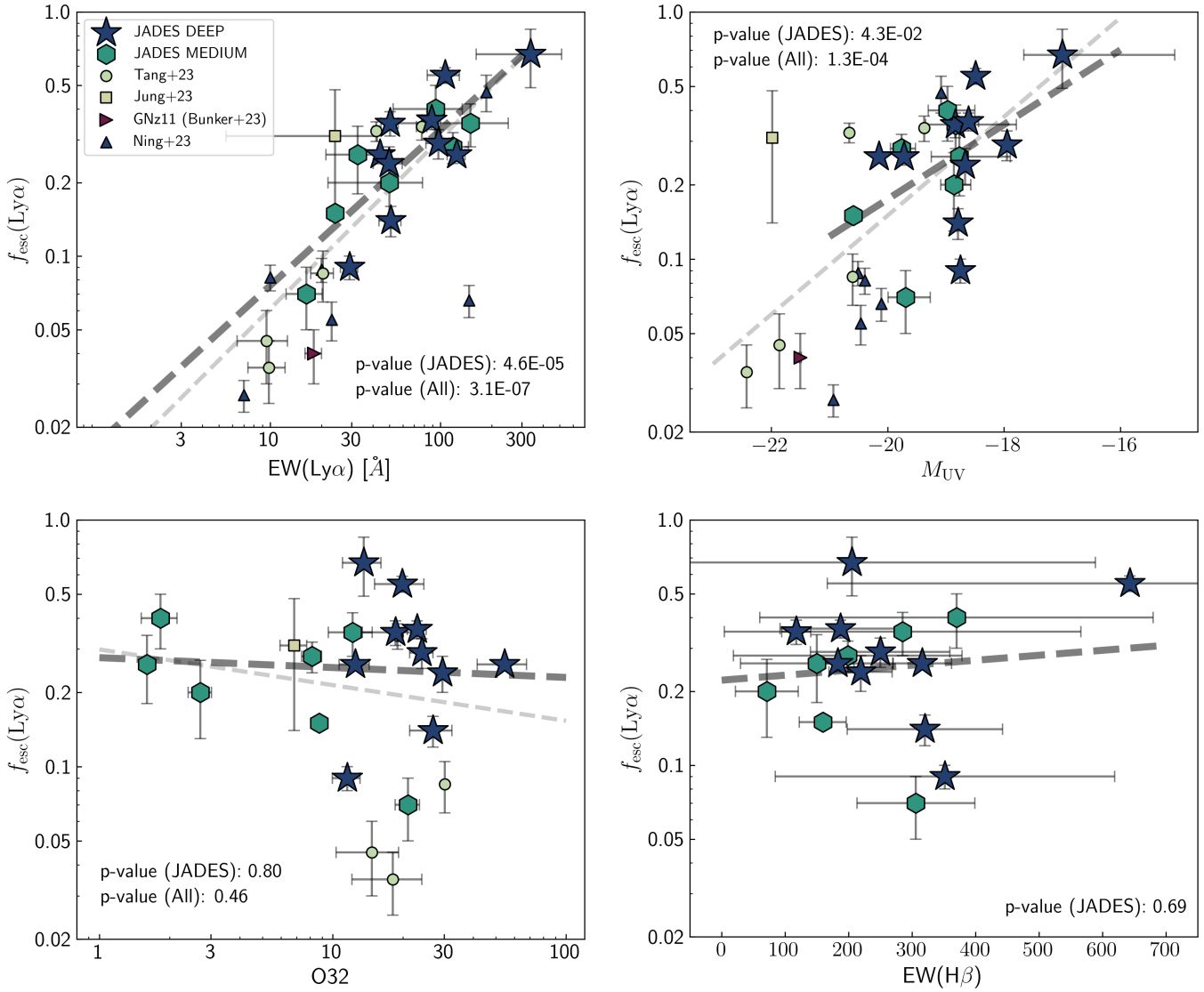

Fig. 7. Dependence of the Lyα escape fraction on EW(Lyα) (top left), $M_{\rm UV}$ (top right), [O III]/[O II] ratio (O32) (bottom left) and EW(Hβ) (bottom right). The correlations follow the same convention as in Fig. 6. Unsurprisingly, we find that $f_{\rm esc}$(Lyα) correlates strongly with EW(Lyα). We also note that UV-faint galaxies show higher $f_{\rm esc}$(Lyα), although this could be attributed purely to the flux limited nature of our spectroscopic survey. We do not find strong correlations between $f_{\rm esc}$(Lyα) and O32 or Hβ strength, although as previously noted we do find that our faint LAEs on average show high O32 ratios and Hβ line strengths.

show $f_{\rm esc}$(Lyα) as a function of redshift, colour-coded by $M_{\rm UV}$ for our LAEs along with others known at $z \gtrsim 5.8$. A decrease in the $f_{\rm esc}$(Lyα) is apparent: the decrease in $f_{\rm esc}$(Lyα) for only the JADES LAEs is less significant with p-value = 0.25, however when including all the LAEs in the redshift of interest from the literature, the decrease is highly significant with p-value = 0.003. Admittedly, the high significance may be driven by the UV magnitude limited nature of these surveys, where Lyα detections from rarer galaxies at the highest redshifts is challenging purely from an observational point of view.

It is also interesting to note that at any given redshift, UV-fainter galaxies exhibit higher $f_{\rm esc}$(Lyα), as we had previously noted. The question that arises from this is, what is truly driving the decrease of $f_{\rm esc}$(Lyα) with redshift? Is the increasing neutrality of the IGM with redshift more dominant than the observational biases associated with being able to only observe UV-bright galaxies at high redshifts from flux limited studies?

To explore this effect, in Fig. 9 we show the $f_{\rm esc}$(Lyα) as a function of redshift for only the UV-brightest galaxies with $M_{\rm UV} < -19.5$ (arbitrarily chosen) to study the evolution in a more flux complete sample of LAEs across a large redshift baseline. This time around, we colour code the data points with Lyα velocity offset, which is a good proxy for the size of the ionized bubble around the LAE.

Figure 9 clearly shows that for UV-bright galaxies at $z > 6$, the decrease in $f_{\rm esc}$(Lyα) is accompanied by an increasing Lyα velocity offset at the highest redshifts, indicating that the decline of EW(Lyα) seen with redshift in UV-bright LAEs is likely driven by the reduction in the sizes of the ionized bubbles traced by the Lyα velocity offset from systemic redshift. This demonstrates that increased IGM attenuation at the highest redshifts is playing an important role in the observed evolution of EW(Lyα), at least within the UV-brightest sample, by attenuating the emergent Lyα flux and the measured $f_{\rm esc}$. The increasing neutral

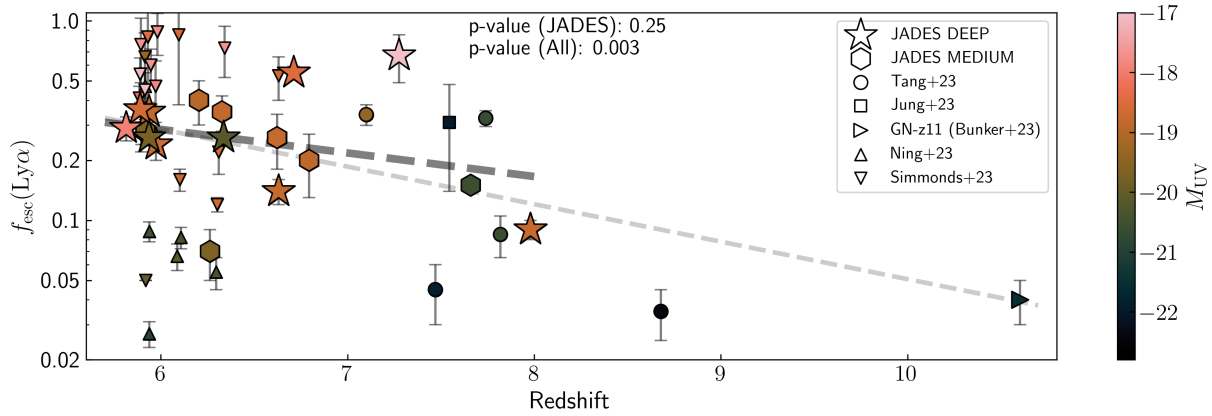

Fig. 8. Evolution of $f_{\rm esc}(\rm Ly\alpha)$ with redshift, colour-coded by the UV magnitude, with significance of the correlations following the convention from Fig. 6. We see a gradual decrease of $f_{\rm esc}(\rm Ly\alpha)$ at increasing redshifts, and at the same redshifts we see a decreasing $f_{\rm esc}(\rm Ly\alpha)$ with increasing UV luminosity as was previously noted. The decrease of $f_{\rm esc}(\rm Ly\alpha)$ with redshift could be driven by both selection biases as well as increasing IGM neutral fraction, and we explore the redshift evolution of only the UV-bright LAEs in Fig. 9.

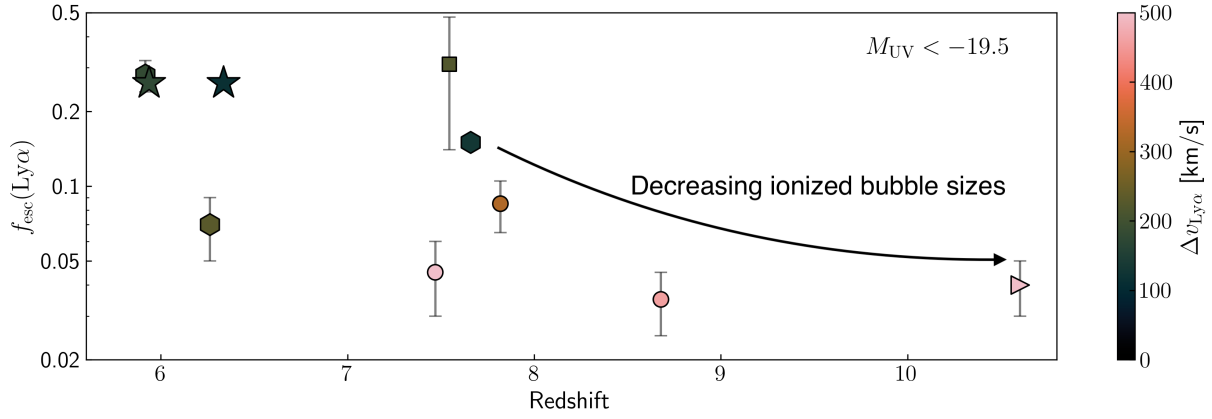

Fig. 9. $f_{\rm esc}(\rm Ly\alpha)$ as a function of redshift for galaxies brighter than $M_{\rm UV} < -19.5$, colour-coded by Lyα velocity offsets. The symbols are the same as in Fig. 8. We find that the Lyα escape fraction also seems to decrease with redshift for brighter galaxies, which is likely driven by the size of the ionized bubbles surrounding each galaxy indicated by the increasing $\Delta v_{\rm Ly\alpha}$ at the highest redshifts, indicating more neutral bubbles around the LAEs. However, increased neutral gas column densities at brighter UV magnitudes may also play a role in redshifting the emergent Lyα emission.

fraction of the IGM from our sample is also clearly seen in the companion paper by Jones et al. (2024).

However, we also note that very high stellar masses for some of the UV-brightest galaxies in the literature sample (e.g. Endsley et al. 2022), accompanied by high neutral gas densities and dust may also attenuate Lyα emission close to the systemic redshift, leading to the same decrease in $f_{\rm esc}(\rm Ly\alpha)$ and increase in the observed Lyα velocity offset. This is similar to the degeneracies between the effect of the ISM vs. the IGM in shaping Lyα properties that was discussed earlier.

Therefore, a combination of selection effects as well as increasingly neutral IGM, which manifests itself as smaller ionized bubbles around LAEs at the highest redshifts play an important role in regulating $f_{\rm esc}(\rm Ly\alpha)$. Estimates on the sizes of ionized regions around JADES LAEs have been presented in a companion paper (Witstok et al. 2024) and offer a powerful probe of the spatial as well as temporal evolution of the IGM neutral fraction in this field.

The comparisons we have presented in this section demonstrate that to use Lyα emission to infer significant LyC photon leakage from galaxies in the reionization era, both high $f_{\rm esc}(\rm Ly\alpha)$ and low Lyα velocity offsets compared to systemic redshift are required. We have found that the dependence of both quantities on other spectroscopic and photometric galaxy properties are filled with complexity and are impacted by observational biases (most importantly the flux limited nature of spectroscopic observations in a field). However, the detection of Lyα emission from a $z > 6$ galaxy is a powerful probe nonetheless at identifying LyC leakage, as has also been noted at lower redshifts (Verhamme et al. 2017; Izotov et al. 2021; Saxena et al. 2022a).

In the next section we attempt to move beyond a simple $f_{\rm esc}(\rm Ly\alpha)$ and use all of the available spectroscopic and photometric indicators to estimate $f_{\rm esc}(\rm LyC)$, which is the quantity that is needed to capture the contribution of galaxies to the reionization budget of the Universe at $z \gtrsim 6$.

5. Implications for LyC photon production, escape and reionization

Although the presence of strong Lyα emission peaking close to the systemic velocity has been used to infer high LyC escape fractions (Verhamme et al. 2015; Izotov et al. 2021; Naidu et al.

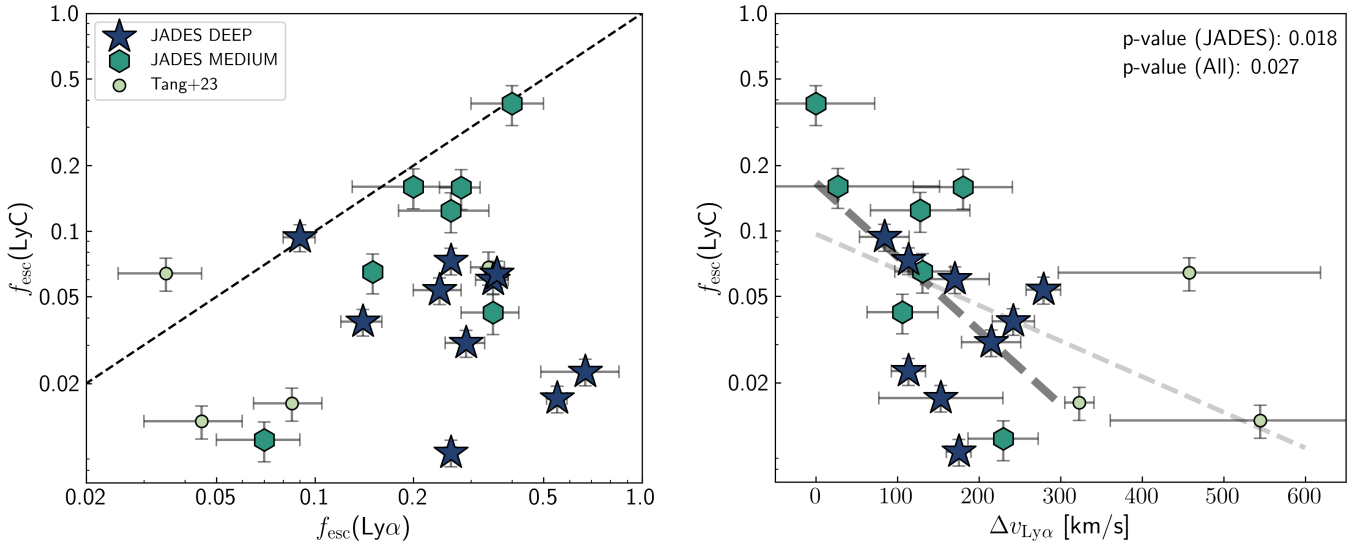

Fig. 10. Comparison of the calculated f_{esc}(LyC) using the relation from Choustikov et al. (2024) with the observed f_{esc}(Lyα) (left, with the one-to-one relation shown as the dashed line) and Lyα velocity offset (right) for LAEs. With the exception of two LAEs from Tang et al. (2023), the f_{esc}(LyC) we infer is always lower than f_{esc}(Lyα), consistent with model predictions (e.g. Maji et al. 2022). Interestingly, one of our faint LAEs has f_{esc}(LyC) > 0.2. We find that qualitatively, f_{esc}(LyC) and Lyα velocity offset anti-correlate, but a low Lyα velocity offset does not necessarily guarantee high f_{esc}(LyC). Similar trends were reported for low redshift LyC leaking galaxies by Izotov et al. (2021).

2022), the physics that control the escape of LyC photons from star-forming galaxies are much more complicated (e.g. Dijkstra 2014; Barrow et al. 2020; Katz et al. 2020; Garel et al. 2021; Maji et al. 2022; Choustikov et al. 2024). The neutral gas content within a galaxy, in particular, can affect the Lyα and LyC photons differently, which combined with the line-of-sight dependence of both Lyα and LyC photon escape can often complicate the inference of LyC photon escape from Lyα alone. For example, one of the most well-studied LyC leakers, Ion1 at $z \approx 3.8$ (Vanzella et al. 2012; Ji et al. 2020) actually does not show any Lyα emission, which demonstrates the complex relationship between Lyα and LyC photons.

Therefore, in this section we fold in other photometric and spectroscopic properties of our faint LAEs to make a more informed inference on the LyC escape fractions. Several observational studies as well as simulations have attempted to connect the leakage of LyC photons to spectroscopic properties. Some of the most exciting observational results linking LyC leakage to galaxy properties are being delivered by the Low-z Lyman Continuum Survey (LzLCS; Flury et al. 2022a,b). State-of-the-art high-resolution cosmological simulations such as SPHINX[20] are also now being used to study the dependence of LyC photon escape on galaxy properties (e.g. Rosdahl et al. 2022; Katz et al. 2023b; Choustikov et al. 2024), which offers much more control on the sample sizes and selection functions when attempting to use observations of galaxy properties to predict f_{esc}(LyC).

Using the SPHINX[20] simulation, Choustikov et al. (2024) specifically focused on observables that trace conditions within galaxies that enable both the production as well as escape of LyC photons. Briefly, these conditions mainly require the galaxies to have (i) relatively high star formation rates (sSFR > 10^{-9} yr^{-1}); (ii) stellar ages in the range 3.5−10 Myr, a time long enough for the first generation of supernovae to have cleared out channels in the ISM for LyC escape, while short enough that UV photons are still being produced in abundance by the stellar population, and (iii) low dust and neutral gas content. Using these criteria, Choustikov et al. (2024) report a six-parameter equation to predict the angle-averaged (and not sight-line dependent) f_{esc}(LyC) based on observed galaxy properties. These parameters include the UV slope, β, dust attenuation $E(B-V)$ (typically measured from the Balmer line decrement), Hβ line luminosity, M_{UV}, R23 and O32.

The predicted f_{esc}(LyC) from Choustikov et al. (2024) have been validated against comprehensive observational efforts to measure f_{esc}(LyC) from low redshift galaxies such as LzLCS (Flury et al. 2022a,b). Each of the individual diagnostics for LyC leakage analysed by Choustikov et al. (2024) agree with what was reported for a handful of candidate LyC leaking galaxies by LzLCS. Further, dependence of f_{esc}(LyC) on one of the most promising indicators, the UV slope (β), was also found to agree with observed trends reported by Chisholm et al. (2022). This validation lends credibility to the LyC leakage predictions and the multi-variate fits derived by Choustikov et al. (2024) to estimate f_{esc}(LyC) for galaxies with good spectroscopic measurements.

Therefore, we use the relationship between f_{esc}(LyC) and galaxy properties derived by Choustikov et al. (2024) to predict f_{esc}(LyC) for our sample of LAEs. The choice of using LyC leakage predictors from Choustikov et al. (2024) over other observational predictors has been made for two main reasons: As Choustikov et al. (2024) demonstrated, single diagnostic based LyC leakage predictors often suffer from scatter, where many ISM/dust/stellar conditions often being necessary but not sufficient for high LyC f_{esc}. These observations may also suffer from sample selection biases, which can be easily overcome when using data from simulations. Secondly, using a multi-variate f_{esc}(LyC) predictor helps encapsulate several competing physical processes within galaxies that eventually result in LyC leakage. With our JWST spectra, these multi-variate measurements are now possible, thereby maximizing the information that can be derived about LyC leakage from our galaxies.

All of the input parameters required to predict f_{esc}(LyC) have been observed for our faint LAEs from JADES, which makes predicting f_{esc}(LyC) using Eq. (4) from Choustikov et al. (2024) relatively straightforward. We note that to predict the

angle-averaged f_{esc}(LyC), the properties of the Lyα emission line, which can often be highly sight-line dependent, are not taken into account by Choustikov et al. (2024) when estimating f_{esc}(LyC) (cf. Maji et al. 2022). The calculated f_{esc}(LyC) for our LAEs are given in Table 4.

In Fig. 10 we show f_{esc}(LyC) calculated using observed galaxy properties compared with f_{esc}(Lyα) measured directly from the spectra (left) and the Lyα velocity offset from the systemic (right) from our faint LAEs as well as those that we calculate using observed quantities from Tang et al. (2023). We find that the predicted f_{esc}(LyC) remains below f_{esc}(Lyα) for all our LAEs, but one LAE from Tang et al. (2023) have higher f_{esc}(LyC) compared to f_{esc}(Lyα).

In general we do not find any strong correlation between f_{esc}(LyC) and f_{esc}(Lyα). We do find that f_{esc}(LyC) significantly anti-correlates with Lyα velocity offset for both our JADES LAEs as well as when brighter LAEs from Tang et al. (2023) are included (Fig. 10, right), but we note that a low ($\lesssim$200 km s^{-1}) Lyα velocity offset does not guarantee a high f_{esc}(LyC) and that there is considerable scatter in the plot. From a sample of low redshift LyC leakers, Izotov et al. (2021) also found that f_{esc}(LyC) tends to always be lower than f_{esc}(Lyα), and that f_{esc}(LyC) weakly anti-correlates with Lyα velocity offset from systemic, consistent with our findings.

We do, however, note the lack of any LAE with high velocity offsets showing high f_{esc}(LyC), which seems to suggest that low Lyα velocity offsets are a necessary but not a sufficient condition to enable high LyC photon escape, mainly tracing the absence of high column density neutral gas, and that galaxies that show large Lyα velocity offsets compared to systemic likely trace highly dense neutral gas conditions, which may not be conducive for significant LyC escape fractions.

Before assessing the co-dependence of ionizing photon production and escape from our faint LAEs, we note that when calculating ξ_{ion} for our LAEs using Eq. (2) in Sect. 2.8 we assumed f_{esc}(LyC) to be zero. However, with f_{esc}(LyC) predictions for our LAEs, we now calculate ξ_{ion}^{corr}, which is corrected for the fraction of ionizing photons that escape out of the galaxy, thereby not contributing towards line emission. In this section going forward, we use the corrected ξ_{ion} value, ξ_{ion}^{corr}.

We now explore the dependence of f_{esc}(LyC) on the corrected ionizing photon production efficiencies in Fig. 11. We find that sources with the highest f_{esc}(LyC) do not necessarily show high values of ξ_{ion}^{corr}. Interestingly, there is am anti-correlation between the two quantities that seems significant based on the p-values, which may be not be entirely unexpected. When non-negligible fractions of ionizing photons begin escaping from the galaxy, there are fewer photons available to produce the Balmer line (as well as strong nebular line) emission (e.g. Topping et al. 2022). This would lead to low ξ_{ion}^{corr} values inferred when simply assuming Case-B recombination, which can consistently explain this observed mild anti-correlation.

Another important effect that may be driving the scatter between f_{esc}(LyC) and ξ_{ion}^{corr} could be the expected time delays between significant production of ionizing photons and the emergence of escape channels that facilitate the escape of those photons. As noted in Choustikov et al. (2024; but see also Barrow et al. 2020; Katz et al. 2020), for a burst of star formation it is not up until ~3.5 Myr since the starburst is triggered that supernovae begin to clear channels in the ISM to allow significant LyC photon escape. Very early on in the starburst, there is a very high production rate of ionizing photons, but these photons are unable to escape out of the H II regions. Therefore, the age of starburst and the time delay between the peak of ionizing photon production and the emergence of escape channels may lead to the observed scatter.

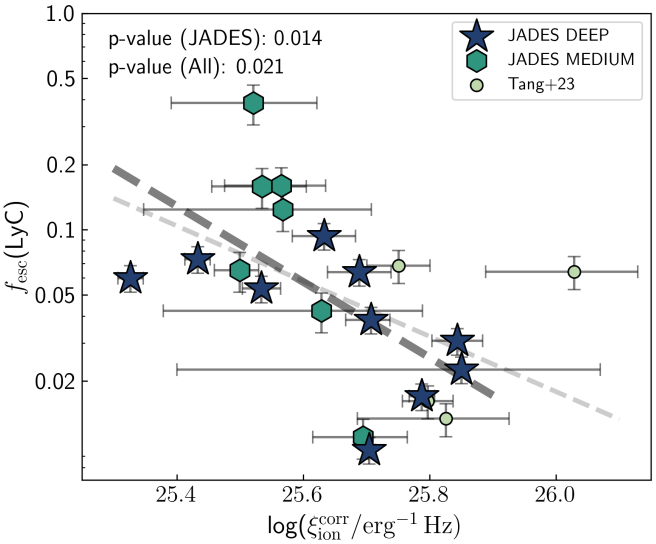

Fig. 11. Corrected ξ_{ion} vs. f_{esc}(LyC) calculated using the multi-parameter fit as described in the text. We find that LAEs that show higher f_{esc}(LyC) have lower measured ξ_{ion} compared to the sample average, which implies that a significant fraction of escaping ionizing photons will lead to decreased Balmer (and potentially nebular) line strengths at a given star formation rate (e.g. Topping et al. 2022). Additionally, this lack of correlation may also arise due to a time delay between the production and escape of ionizing photons from galaxies, whereby intense star formation activity that produces ionizing photons needs time to clear out channels to also facilitate LyC escape, as has been reported from several high-resolution simulations (e.g. Barrow et al. 2020; Katz et al. 2020; Choustikov et al. 2024).

Finally, we explore the dependence of the product of the ionizing photon production efficiency and the ionizing photon escape fraction (f_{esc}(LyC) $\times\,\xi_{ion}^{corr}$), which is an important quantity needed to assess the contribution of individual star-forming galaxies to the reionization budget of the Universe, with UV magnitude, EW of Lyα emission and its evolution with redshift. To overcome any potential sample selection biases, we restrict our analysis only to the JADES LAEs here, for which the selection functions and completeness is fairly well understood. The average ionizing photon output from our JADES LAEs is $\log(f_{esc}(\mathrm{LyC}) \times \xi_{ion}^{corr}/\mathrm{erg^{-1}\,Hz}) = 24.49^{+0.29}_{-0.39}$. This measurement is in agreement with that reported by Meyer et al. (2019) for faint galaxy populations in the redshift range $4.5 < z < 6.2$. The correlations between f_{esc}(LyC) $\times\,\xi_{ion}^{corr}$ and the above-mentioned quantities are shown in Fig. 12 and are discussed below.

We begin by assessing the dependence of $\log(f_{esc}(\mathrm{LyC}) \times \xi_{ion}^{corr})$ on UV magnitude, finding that it increases very mildly with decreasing M_{UV} as shown in Fig. 12 (top left), following the linear relation:

$$\log\left(\frac{f_{esc} \times \xi_{ion}^{corr}}{\mathrm{erg^{-1}\,Hz}}\right) = 0.047\,(\pm0.014)\,M_{UV} + 25.27\,(\pm5.16). \quad (3)$$

This lack of strong correlation for LAEs clearly disfavours enhanced ionizing photon output from UV-fainter LAEs, and may have important consequences for models of reionization.

We further find that the ionizing photon output from LAEs also remains roughly constant over a range of EW(Lyα), best fit

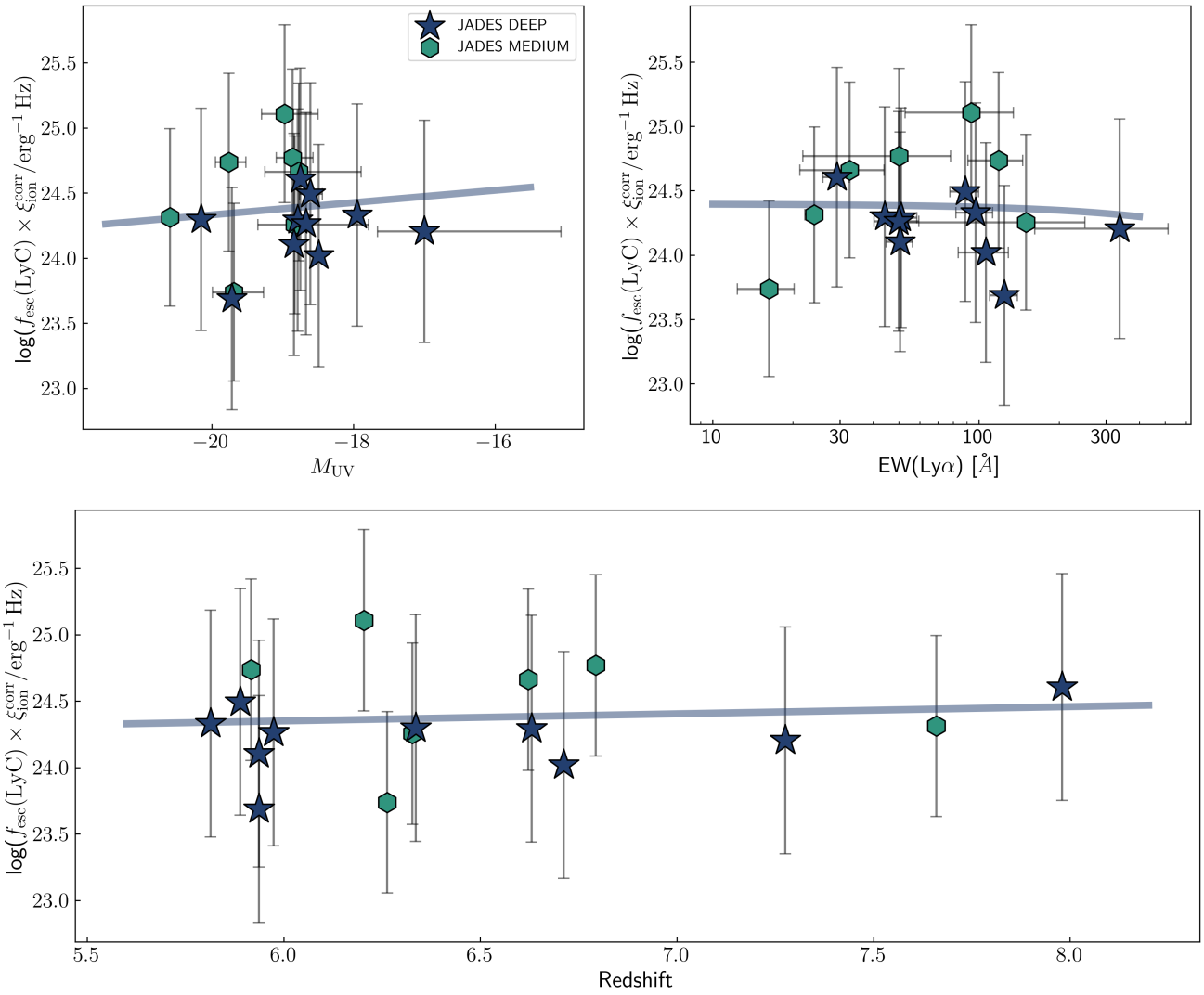

Fig. 12. Dependence of the ionizing photon output from galaxies (that is $f_{\rm esc}({\rm LyC}) \times \xi_{\rm ion}$) as a function of UV magnitude (left) and Lyα equivalent width (right). The best-fitting linear relations are shown as blue lines (with considerable scatter in the relation, which is not shown to preserve clarity). Overall, we do not find any strong dependence of the ionizing photon output on either the UV magnitude of the Lyα strength. The ionizing photon output is key to quantifying the role of star-forming galaxies in contributing towards the reionization budget at $z > 6$.

with the linear relation:

$$\log\left(\frac{f_{\rm esc} \times \xi_{\rm ion}^{\rm corr}}{\rm erg^{-1}\,Hz}\right) = -2.5 \times 10^{-4}\,(\pm 1.9 \times 10^{-6})\left(\frac{\rm EW(Ly\alpha)}{\rm \AA}\right) + 24.39\,(\pm 0.02). \quad (4)$$

The little to no dependence of $\log(f_{\rm esc} \times \xi_{\rm ion})$ on the equivalent width of Lyα emission is shown in Fig. 12 (top right; note that the x-axis is in log scale), implying that purely the observed Lyα line strength is not a good independent indicator of the ionizing photon output from LAEs in the epoch of reionization. The added attenuation by the neutral IGM along the line of sight at $z > 6$ and the inherent difficulty in disentangling the effects of the IGM and ISM/CGM at these redshifts likely contributes to the Lyα line strength not being a robust tracer of the ionizing photon output.

Finally, we derive the dependence of the ionizing photon output of our LAEs with redshift, finding the best-fitting relation:

$$\log\left(\frac{f_{\rm esc} \times \xi_{\rm ion}}{\rm erg^{-1}\,Hz}\right) = 0.053\,(\pm 0.025)\,z + 24.027\,(\pm 1.050). \quad (5)$$

We find that the ionizing photon output of LAEs shows a mild increase with redshift as shown in Fig. 12 (bottom). This is consistent with a picture whereby younger galaxies may be able to achieve higher ionizing photon production efficiencies, but the relatively mild evolution is also consistent with a picture whereby the production and escape of ionizing photons is dictated by physical processes that operate on much-shorter timescales (that is intense star formation or SNe activity), which cannot be captured via a strong trend with redshift.

The best-fitting relations of ionizing photon output with UV magnitude Lyα EW and redshift can be used to estimate the total number of ionizing photons contributed by LAEs at a given redshift, depending on the space density of LAEs. Since the increasing neutrality of the IGM makes it impossible to obtain a complete Lyα luminosity function at $z > 6$, certain assumptions about the evolution of the Lyα luminosity function may need to be made (see Matthee et al. 2022, for example).

Alternatively, if a good handle on the Lyα emitter fraction (unaffected by the IGM attenuation) can be obtained at $z > 6$ by extrapolating from fractions measured at lower redshifts (e.g.

Santos et al. 2020), then our best-fitting relations can also be used to estimate the total ionizing photon contribution towards the reionization budget from LAEs at $z > 6$. Any dependence of the LAE fraction on UV magnitude must also be taken into account for this calculation (see Jones et al. 2024).

6. Conclusions

In this study we have presented detailed properties of 17 faint Lyα emitting galaxies at $z > 5.8$ from the JWST Advanced Deep Extragalactic Survey (JADES) Deep and Medium Tier NIRSpec MSA surveys. These new Lyα emitters, spanning absolute UV magnitudes of -17.0 to -20.6, are generally fainter compared to LAEs that were previously known in or near the epoch of reionization, opening up a new window into studying the properties of faint galaxies that reside within ionized bubbles in the reionization era.

Using measurements directly from the low resolution (R100) PRISM as well as medium resolution (R1000) grating spectra, we report the detection of other rest-frame optical emission lines such as [O II], Hβ, [O III] and Hα. The detection of these lines enables a reliable measure of their spectroscopic redshift against which the velocity offsets of Lyα emission can be accurately measured. In general, these LAEs have blue rest-UV spectral slopes (-2.1 to -2.7) and little to no dust measured from Balmer decrements.

Using rest-optical line ratios, we find that our LAEs appear to be metal poor with high ionization parameters, properties that are typical of JWST-detected faint star-forming galaxies at $z > 6$. These properties combined with steep UV slopes and no dust indicate that all of our LAEs are young, star-forming systems. We further measure the ionizing photon production efficiencies ($\xi_{\rm ion}$) directly from Balmer line emission and find that our LAEs on average have $\log(\xi_{\rm ion}/{\rm Hz\,erg^{-1}}) \approx 25.56$, which does not seem to evolve strongly with redshift. We also do not find a strong dependence of $\xi_{\rm ion}$ on the strength of Lyα emission.

Using the Lyα escape fraction (calculated using Balmer line emission) and the velocity offset of the peak of the Lyα line compared to systemic redshift, we study the galaxy properties that govern the escape of Lyα photons from reionization era galaxies. We note that the escape fraction of Lyα photons is anti-correlated with its velocity offset from systemic, and is strongly correlated with Lyα equivalent width, consistent with expectations from Lyα emission models as well as high-resolution galaxy simulations employing radiative transfer to track the escape of Lyα emission.

We also find that LAEs that are fainter in the UV show higher Lyα escape fractions, although this could be attributed to the flux limited nature of our spectroscopic surveys. We do not find strong correlations between Lyα escape fraction or velocity offset with key ISM indicators such as [O III]/[O II] ratios or Hβ equivalent widths. We conclude that the escape of Lyα emission is a complicated process, and may not necessarily depend strongly on the state of the ISM and stellar populations at any given time, especially at $z > 6$ when the IGM attenuation also plays an important role.

We find a gradual decrease in Lyα escape fractions with redshift, indicative of increasing IGM attenuation in diminishing Lyα strengths at the highest redshifts. By making a UV cut to remove selection effects, we find that the Lyα escape fraction still evolves weakly with redshift, but the escaping Lyα emission is considerably more offset compared to systemic velocity at the highest redshifts, indicative of decreasing ionized fractions and sizes of the bubbles that must surround these LAEs.

Making use of several photometric and spectroscopic indicators for our LAEs, we then predict escape fractions of hydrogen ionizing Lyman continuum photons. We find that with the exception of one LAE in our sample, the LyC escape fraction is always lower than the Lyα escape fraction, with no significant correlations between the two. We also do not find any significant correlation between LyC escape fraction and $\xi_{\rm ion}$, which can likely explained by the reduced Balmer line emission in the presence of significant ionizing photon escape or by time delays between the production and escape of ionizing photons.

By combining the production and escape of LyC photons (that is $f_{\rm esc} \times \xi_{\rm ion}$), we find that the quantity that is actually responsible for delivering ionizing photons from the galaxies to the IGM remains relatively consistent across UV magnitudes and EW(Lyα), but increases gradually with redshift. Using these dependencies and assumptions about the Lyα emitter fraction at any given redshift, more realistic models of reionization can be constructed.

Deeper and wider spectroscopic surveys in the future will help expand the samples of known LAEs in the reionization era. The availability of other spectroscopic indicators tracing the nature of stellar populations, ISM ionization and chemical conditions would be key to assess the role of Lyα emitting galaxies in driving cosmic reionization, helping build more realistic models charting the reionization history of the Universe.

Acknowledgements. We would like to thank the referee for constructive comments that helped improve the quality of this manuscript. AS thanks Harley Katz, Richard Ellis, Jorryt Matthee and Anne Verhamme for insightful discussions. AS, AJB, GCJ, AJC and JC acknowledge funding from the "FirstGalaxies" Advanced Grant from the European Research Council (ERC) under the European Union's Horizon 2020 research and innovation programme (Grant agreement No. 789056). JW, RM, MC, TJL, LS and JS acknowledge support by the Science and Technology Facilities Council (STFC), ERC Advanced Grant 695671 "QUENCH". JW also acknowledges support from the Fondation MERAC. SA acknowledges support from the research project PID2021-127718NB- I00 of the Spanish Ministry of Science and Innovation/State Agency of Research (MICIN/AEI). RB acknowledges support from an STFC Ernest Rutherford Fellowship (ST/T003596/1). KB acknowledges support from the Australian Research Council Centre of Excellence for All Sky Astrophysics in 3 Dimensions (ASTRO 3D), through project number CE170100013. SC acknowledges support by European Union's HE ERC Starting Grant No. 101040227 – "WINGS". ECL acknowledges support of an STFC Webb Fellowship (ST/W001438/1). DJE is supported as a Simons Investigator and by JWST/NIRCam contract to the University of Arizona, NAS5- 02015. BDJ, BER and MR acknowledge support from the NIRCam Science Team contract to the University of Arizona, NAS5-02015. RS acknowledges support from a STFC Ernest Rutherford Fellowship (ST/S004831/1). The work of CCW is supported by NOIR-Lab, which is managed by the Association of Universities for Research in Astronomy (AURA) under a cooperative agreement with the National Science Foundation. This work is based on observations made with the NASA/ESA/CSA *James Webb* Space Telescope. The data were obtained from the Mikulski Archive for Space Telescopes at the Space Telescope Science Institute, which is operated by the Association of Universities for Research in Astronomy, Inc., under NASA contract NAS 5-03127 for JWST. These observations are associated with program #1180 and #1210.

References

Aihara, H., Allende Prieto, C., An, D., et al. 2011, ApJS, 193, 29
Ajiki, M., Taniguchi, Y., Fujita, S. S., et al. 2003, AJ, 126, 2091
Arellano-Córdova, K. Z., Berg, D. A., Chisholm, J., et al. 2022, ApJ, 940, L23
Atek, H., Kunth, D., Hayes, M., Östlin, G., & Mas-Hesse, J. M. 2008, A&A, 488, 491
Barrow, K. S. S., Robertson, B. E., Ellis, R. S., et al. 2020, ApJ, 902, L39
Böker, T., Beck, T. L., Birkmann, S. M., et al. 2023, PASP, 135, 038001
Bolan, P., Lemaux, B. C., Mason, C., et al. 2022, MNRAS, 517, 3263
Bosman, S. E. I., Davies, F. B., Becker, G. D., et al. 2022, MNRAS, 514, 55
Bouwens, R. J., Smit, R., Schouws, S., et al. 2022, ApJ, 931, 160
Bunker, A. J., Cameron, A. J., Curtis-Lake, E., et al. 2023a, A&A, submitted, [arXiv:2306.02467]
Bunker, A. J., Saxena, A., Cameron, A. J., et al. 2023b, A&A, 677, A88
Calzetti, D., Kinney, A. L., & Storchi-Bergmann, T. 1994, ApJ, 429, 582
Cameron, A. J., Saxena, A., Bunker, A. J., et al. 2023, A&A, 677, A115
Carniani, S., Maiolino, R., Pallottini, A., et al. 2017, A&A, 605, A42
Carniani, S., Maiolino, R., Smit, R., & Amorín, R. 2018, ApJ, 854, L7

Caruana, J., Bunker, A. J., Wilkins, S. M., et al. 2012, MNRAS, 427, 3055
Caruana, J., Bunker, A. J., Wilkins, S. M., et al. 2014, MNRAS, 443, 2831
Castellano, M., Pentericci, L., Cupani, G., et al. 2022, A&A, 662, A115
Chisholm, J., Saldana-Lopez, A., Flury, S., et al. 2022, MNRAS, 517, 5104
Choustikov, N., Katz, H., Saxena, A., et al. 2024, MNRAS, in press, https://doi.org/10.1093/mnras/stae776
Cuby, J. G., Le Fèvre, O., McCracken, H., et al. 2003, A&A, 405, L19
Curti, M., D'Eugenio, F., Carniani, S., et al. 2023, MNRAS, 518, 425
Curtis-Lake, E., Carniani, S., Cameron, A., et al. 2023, Nat. Astron., 7, 622
Dayal, P., & Ferrara, A. 2018, Phys. Rep., 780, 1
Dijkstra, M. 2014, PASA, 31, e040
Dijkstra, M., Haiman, Z., & Spaans, M. 2006, ApJ, 649, 14
Eisenstein, D. J., Willott, C., Alberts, S., et al. 2023, ApJ, submitted, [arXiv:2306.02465]
Endsley, R., Stark, D. P., Bouwens, R. J., et al. 2022, MNRAS, 517, 5642
Endsley, R., Stark, D. P., Whitler, L., et al. 2023, MNRAS, 524, 2312
Erb, D. K., Steidel, C. C., Trainor, R. F., et al. 2014, ApJ, 795, 33
Fan, X., Carilli, C. L., & Keating, B. 2006, ARA&A, 44, 415
Feltre, A., Maseda, M. V., Bacon, R., et al. 2020, A&A, 641, A118
Ferruit, P., Jakobsen, P., Giardino, G., et al. 2022, A&A, 661, A81
Fletcher, T. J., Tang, M., Robertson, B. E., et al. 2019, ApJ, 878, 87
Flury, S. R., Jaskot, A. E., Ferguson, H. C., et al. 2022a, ApJS, 260, 1
Flury, S. R., Jaskot, A. E., Ferguson, H. C., et al. 2022b, ApJ, 930, 126
Fujimoto, S., Arrabal Haro, P., Dickinson, M., et al. 2023, ApJ, 949, L25
Fuller, S., Lemaux, B. C., Bradač, M., et al. 2020, ApJ, 896, 156
Furlanetto, S. R., Zaldarriaga, M., & Hernquist, L. 2006, MNRAS, 365, 1012
Furusawa, H., Kashikawa, N., Kobayashi, M. A. R., et al. 2016, ApJ, 822, 46
Garel, T., Blaizot, J., Rosdahl, J., et al. 2021, MNRAS, 504, 1902
Giavalisco, M., Ferguson, H. C., Koekemoer, A. M., et al. 2004, ApJ, 600, L93
Gordon, K. D., Clayton, G. C., Misselt, K. A., Landolt, A. U., & Wolff, M. J. 2003, ApJ, 594, 279
Haiman, Z. 2002, ApJ, 576, L1
Harikane, Y., Ouchi, M., Shibuya, T., et al. 2018, ApJ, 859, 84
Hashimoto, T., Inoue, A. K., Mawatari, K., et al. 2019, PASJ, 71, 71
Hayes, M. J., & Scarlata, C. 2023, ApJ, 954, L14
Hayes, M., Östlin, G., Schaerer, D., et al. 2013, ApJ, 765, L27
Hayes, M. J., Runnholm, A., Scarlata, C., Gronke, M., & Rivera-Thorsen, T. E. 2023, MNRAS, 520, 5903
Hoag, A., Bradač, M., Huang, K., et al. 2019, ApJ, 878, 12
Inoue, A. K., Shimizu, I., Iwata, I., & Tanaka, M. 2014, MNRAS, 442, 1805
Izotov, Y. I., Schaerer, D., Worseck, G., et al. 2020, MNRAS, 491, 468
Izotov, Y. I., Worseck, G., Schaerer, D., et al. 2021, MNRAS, 503, 1734
Jakobsen, P., Ferruit, P., Alves de Oliveira, C., et al. 2022, A&A, 661, A80
Ji, Z., Giavalisco, M., Vanzella, E., et al. 2020, ApJ, 888, 109
Jones, G. C., Bunker, A. J., Saxena, A., et al. 2024, A&A, 683, A238
Jung, I., Finkelstein, S. L., Arrabal Haro, P., et al. 2023, ApJ, submitted, [arXiv:2304.05385]
Katz, H., Ďurovčíková, D., Kimm, T., et al. 2020, MNRAS, 498, 164
Katz, H., Saxena, A., Cameron, A. J., et al. 2023a, MNRAS, 518, 592
Katz, H., Saxena, A., Rosdahl, J., et al. 2023b, MNRAS, 518, 270
Keating, L. C., Weinberger, L. H., Kulkarni, G., et al. 2020, MNRAS, 491, 1736
Kerutt, J., Wisotzki, L., Verhamme, A., et al. 2022, A&A, 659, A183
Knudsen, K. K., Richard, J., Kneib, J.-P., et al. 2016, MNRAS, 462, L6
Kuhlen, M., & Faucher-Giguère, C.-A. 2012, MNRAS, 423, 862
Kusakabe, H., Blaizot, J., Garel, T., et al. 2020, A&A, 638, A12
Laporte, N., Nakajima, K., Ellis, R. S., et al. 2017, ApJ, 851, 40
Laursen, P., Sommer-Larsen, J., & Andersen, A. C. 2009, ApJ, 704, 1640
Luridiana, V., Morisset, C., & Shaw, R. A. 2015, A&A, 573, A42
Mainali, R., Kollmeier, J. A., Stark, D. P., et al. 2017, ApJ, 836, L14
Maiolino, R., Carniani, S., Fontana, A., et al. 2015, MNRAS, 452, 54
Maji, M., Verhamme, A., Rosdahl, J., et al. 2022, A&A, 663, A66
Malhotra, S., & Rhoads, J. E. 2006, ApJ, 647, L95
Mascia, S., Pentericci, L., Calabrò, A., et al. 2023, A&A, 672, A155
Maseda, M. V., Bacon, R., Lam, D., et al. 2020, MNRAS, 493, 5120
Mason, C. A., & Gronke, M. 2020, MNRAS, 499, 1395
Mason, C. A., Treu, T., Dijkstra, M., et al. 2018, ApJ, 856, 2
Matthee, J., Sobral, D., Best, P., et al. 2017a, MNRAS, 471, 629
Matthee, J., Sobral, D., Boone, F., et al. 2017b, ApJ, 851, 145
Matthee, J., Sobral, D., Boogaard, L. A., et al. 2019, ApJ, 881, 124
Matthee, J., Sobral, D., Gronke, M., et al. 2020, MNRAS, 492, 1778
Matthee, J., Naidu, R. P., Pezzulli, G., et al. 2022, MNRAS, 512, 5960
Meyer, R. A., Bosman, S. E. I., Kakiichi, K., & Ellis, R. S. 2019, MNRAS, 483, 19
Miralda-Escudé, J. 1998, ApJ, 501, 15
Naidu, R. P., Forrest, B., Oesch, P. A., Tran, K.-V. H., & Holden, B. P. 2018, MNRAS, 478, 791
Naidu, R. P., Matthee, J., Oesch, P. A., et al. 2022, MNRAS, 510, 4582
Nakajima, K., Ellis, R. S., Robertson, B. E., Tang, M., & Stark, D. P. 2020, ApJ, 889, 161
Nakajima, K., Ouchi, M., Isobe, Y., et al. 2023, ApJS, 269, 33
Neufeld, D. A. 1990, ApJ, 350, 216
Ning, Y., Cai, Z., Jiang, L., et al. 2023, ApJ, 944, L1
Oesch, P. A., van Dokkum, P. G., Illingworth, G. D., et al. 2015, ApJ, 804, L30
Oke, J. B., & Gunn, J. E. 1983, ApJ, 266, 713
Orlitová, I., Verhamme, A., Henry, A., et al. 2018, A&A, 616, A60
Osterbrock, D. E. 1989, Astrophysics of Gaseous Nebulae and Active Galactic Nuclei (University Science Books)
Ouchi, M., Ellis, R., Ono, Y., et al. 2013, ApJ, 778, 102
Pahl, A. J., Shapley, A., Steidel, C. C., Chen, Y., & Reddy, N. A. 2021, MNRAS, 505, 2447
Pentericci, L., Fontana, A., Vanzella, E., et al. 2011, ApJ, 743, 132
Pentericci, L., Carniani, S., Castellano, M., et al. 2016, ApJ, 829, L11
Pentericci, L., McLure, R. J., Garilli, B., et al. 2018a, A&A, 616, A174
Pentericci, L., Vanzella, E., Castellano, M., et al. 2018b, A&A, 619, A147
Planck Collaboration VI. 2020, A&A, 641, A6
Prieto-Lyon, G., Mason, C., Mascia, S., et al. 2023a, ApJ, 956, 136
Prieto-Lyon, G., Strait, V., Mason, C. A., et al. 2023b, A&A, 672, A186
Rieke, M. J., Kelly, D. M., Misselt, K., et al. 2023a, PASP, 135, 028001
Rieke, M. J., Robertson, B., Tacchella, S., et al. 2023b, ApJS, 269, 16
Roberts-Borsani, G. W., Bouwens, R. J., Oesch, P. A., et al. 2016, ApJ, 823, 143
Robertson, B. E. 2022, ARA&A, 60, 121
Robertson, B. E., Furlanetto, S. R., Schneider, E., et al. 2013, ApJ, 768, 71
Robertson, B. E., Ellis, R. S., Furlanetto, S. R., & Dunlop, J. S. 2015, ApJ, 802, L19
Robertson, B. E., Tacchella, S., Johnson, B. D., et al. 2023, Nat. Astron., 7, 611
Rosdahl, J., Blaizot, J., Katz, H., et al. 2022, MNRAS, 515, 2386
Roy, N., Henry, A., Treu, T., et al. 2023, ApJ, 952, L14
Sanders, R. L., Shapley, A. E., Topping, M. W., Reddy, N. A., & Brammer, G. B. 2023, ApJ, 955, 54
Sandles, L., D'Eugenio, F., Maiolino, R., et al. 2023, A&A, submitted, [arXiv:2306.03931]
Santos, S., Sobral, D., Matthee, J., et al. 2020, MNRAS, 493, 141
Saxena, A., Ellis, R. S., Förster, P. U., et al. 2021, MNRAS, 505, 4798
Saxena, A., Cryer, E., Ellis, R. S., et al. 2022a, MNRAS, 517, 1098
Saxena, A., Pentericci, L., Ellis, R. S., et al. 2022b, MNRAS, 511, 120
Saxena, A., Robertson, B. E., Bunker, A. J., et al. 2023, A&A, 678, A68
Shivaei, I., Reddy, N., Rieke, G., et al. 2020, ApJ, 899, 117
Simmonds, C., Tacchella, S., Maseda, M., et al. 2023, MNRAS, 523, 5468
Simmonds, C., Tacchella, S., Hainline, K., et al. 2024, MNRAS, 527, 6139
Smith, A., Ma, X., Bromm, V., et al. 2019, MNRAS, 484, 39
Sobral, D., Matthee, J., Darvish, B., et al. 2015, ApJ, 808, 139
Stark, D. P. 2016, ARA&A, 54, 761
Stark, D. P., Richard, J., Charlot, S., et al. 2015, MNRAS, 450, 1846
Stark, D. P., Ellis, R. S., Charlot, S., et al. 2017, MNRAS, 464, 469
Steidel, C. C., Giavalisco, M., Dickinson, M., & Adelberger, K. L. 1996, AJ, 112, 352
Sun, F., Egami, E., Pirzkal, N., et al. 2023, ApJ, 953, 53
Tacchella, S., Johnson, B. D., Robertson, B. E., et al. 2023, MNRAS, 522, 6236
Tang, M., Stark, D. P., Chen, Z., et al. 2023, MNRAS, 526, 1657
Topping, M. W., Stark, D. P., Endsley, R., et al. 2022, ApJ, 941, 153
Trapp, A. C., Furlanetto, S. R., & Davies, F. B. 2023, MNRAS, 524, 5891
Trump, J. R., Arrabal Haro, P., Simons, R. C., et al. 2023, ApJ, 945, 35
Vanzella, E., Pentericci, L., Fontana, A., et al. 2011, ApJ, 730, L35
Vanzella, E., Guo, Y., Giavalisco, M., et al. 2012, ApJ, 751, 70
Verhamme, A., Schaerer, D., & Maselli, A. 2006, A&A, 460, 397
Verhamme, A., Orlitová, I., Schaerer, D., & Hayes, M. 2015, A&A, 578, A7
Verhamme, A., Orlitová, I., Schaerer, D., et al. 2017, A&A, 597, A13
Weinberger, L. H., Haehnelt, M. G., & Kulkarni, G. 2019, MNRAS, 485, 1350
Willott, C. J., Carilli, C. L., Wagg, J., & Wang, R. 2015, ApJ, 807, 180
Witstok, J., Smit, R., Saxena, A., et al. 2024, A&A, 682, A40
Witten, C., Laporte, N., Martin-Alvarez, S., et al. 2024, Nat. Astron., 8, 384
Yang, H., Malhotra, S., Gronke, M., et al. 2017, ApJ, 844, 171
Zackrisson, E., Inoue, A. K., & Jensen, H. 2013, ApJ, 777, 39

[1] Department of Physics, University of Oxford, Denys Wilkinson Building, Keble Road, Oxford OX1 3RH, UK
e-mail: aayush.saxena@physics.ox.ac.uk
[2] Department of Physics and Astronomy, University College London, Gower Street, London WC1E 6BT, UK

[3] Steward Observatory, University of Arizona, 933 N. Cherry Ave., Tucson, AZ 85721, USA
[4] Kavli Institute for Cosmology, University of Cambridge, Madingley Road, Cambridge CB3 0HA, UK
[5] Cavendish Laboratory, University of Cambridge, 19 JJ Thomson Avenue, Cambridge CB3 0HE, UK
[6] Centro de Astrobiología (CAB), CSIC-INTA, Cra. de Ajalvir Km. 4, 28850 Torrejón de Ardoz, Madrid, Spain
[7] Department of Physics and Astronomy, University of Manitoba, Winnipeg MB R3T 2N2, Canada
[8] European Space Agency (ESA), European Space Astronomy Centre (ESAC), Camino Bajo del Castillo s/n, 28692 Villanueva de la Cañada, Madrid, Spain
[9] European Space Agency, ESA/ESTEC, Keplerlaan 1, 2201 AZ, Noordwijk, The Netherlands
[10] Jodrell Bank Centre for Astrophysics, Department of Physics and Astronomy, School of Natural Sciences, The University of Manchester, Manchester M13 9PL, UK
[11] School of Physics, University of Melbourne, Parkville 3010, VIC, Australia
[12] ARC Centre of Excellence for All Sky Astrophysics in 3 Dimensions (ASTRO 3D), Australia
[13] Scuola Normale Superiore, Piazza dei Cavalieri 7, 56126 Pisa, Italy
[14] Sorbonne Université, CNRS, UMR 7095, Institut d'Astrophysique de Paris, 98 bis bd Arago, 75014 Paris, France
[15] European Southern Observatory, Karl-Schwarzschild-Strasse 2, 85748 Garching bei Muenchen, Germany
[16] Centre for Astrophysics Research, Department of Physics, Astronomy and Mathematics, University of Hertfordshire, Hatfield AL10 9AB, UK
[17] Centre for Astrophysics | Harvard & Smithsonian, 60 Garden St., Cambridge, MA 02138, USA
[18] Department of Astronomy, University of Texas, Austin, TX 78712, USA
[19] AURA for European Space Agency, Space Telescope Science Institute, 3700 San Martin Drive., Baltimore, MD 21210, USA
[20] Max-Planck-Institut für Astronomie, Königstuhl 17, 69117 Heidelberg, Germany
[21] Department of Astronomy and Astrophysics, University of California, Santa Cruz, 1156 High Street, Santa Cruz, CA 95064, USA
[22] Astrophysics Research Institute, Liverpool John Moores University, 146 Brownlow Hill, Liverpool L3 5RF, UK
[23] NSF's National Optical-Infrared Astronomy Research Laboratory, 950 North Cherry Avenue, Tucson, AZ 85719, USA
[24] NRC Herzberg, 5071 West Saanich Rd, Victoria, BC V9E 2E7, Canada

Appendix A: 1D spectra of LAEs

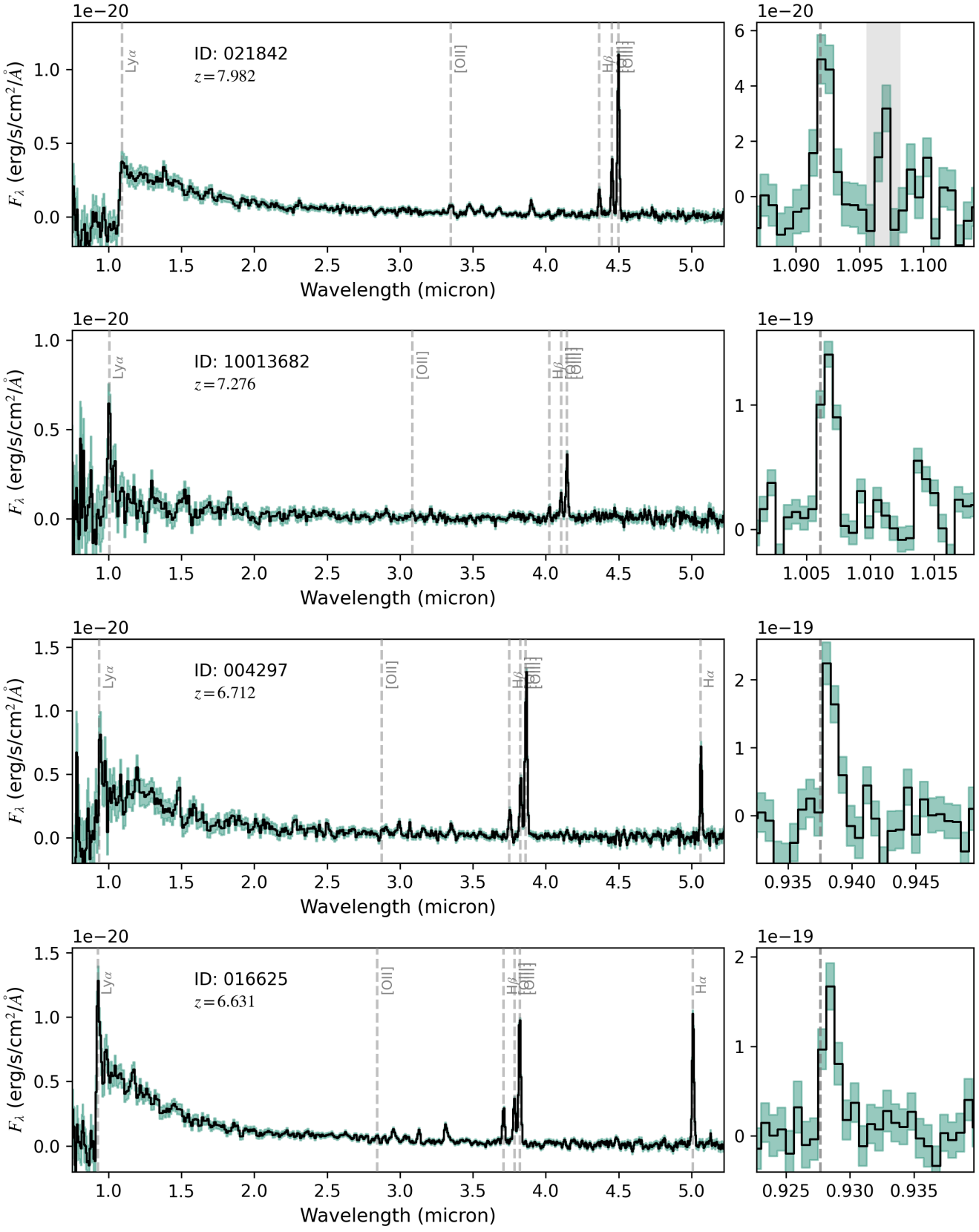

Fig. A.1. 1D spectra of LAEs from PRISM (R100) with a zoom-in on Lyα emission from G140M (R1000).

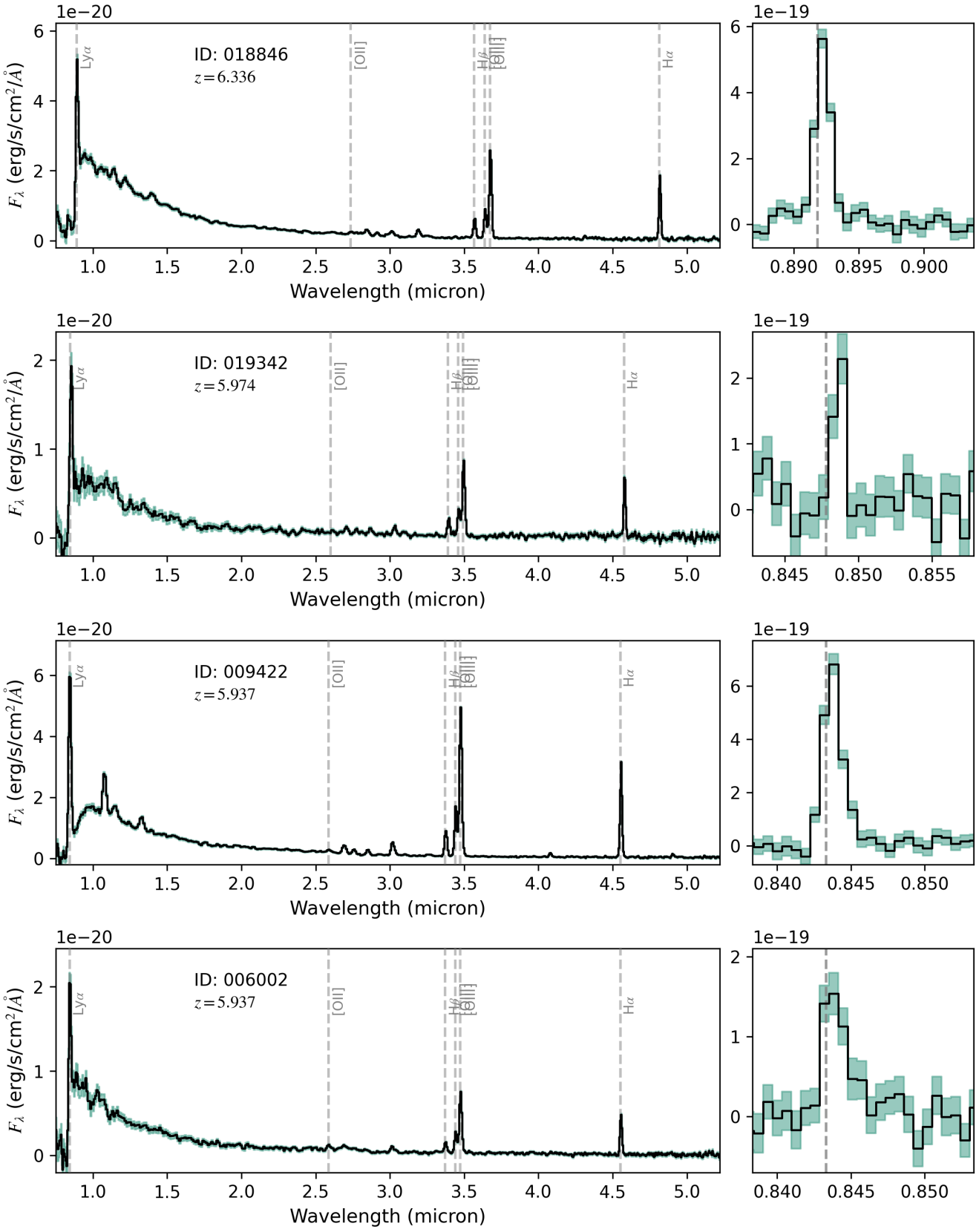

Fig. A.1. continued.

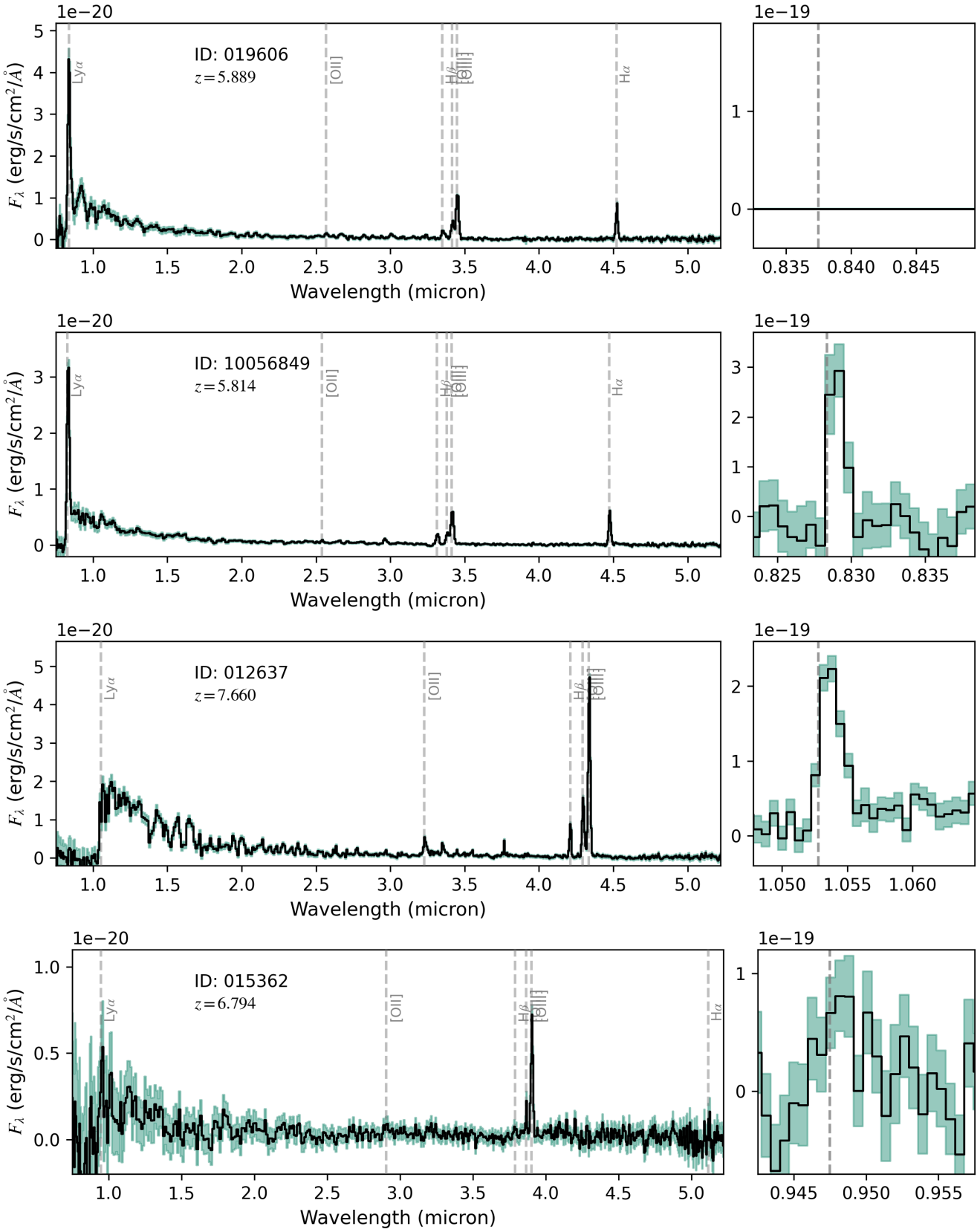

Fig. A.1. continued.

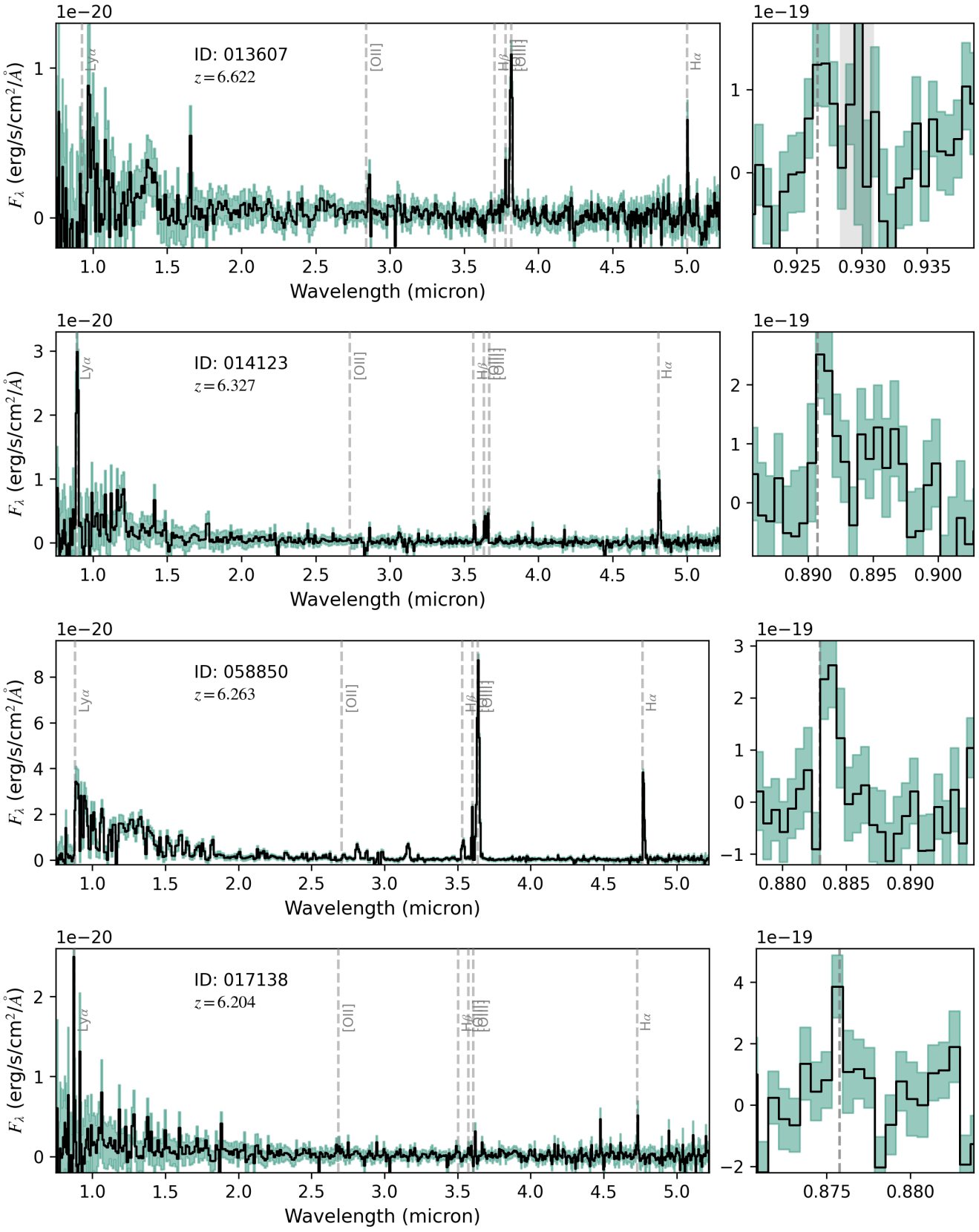

Fig. A.1. continued.

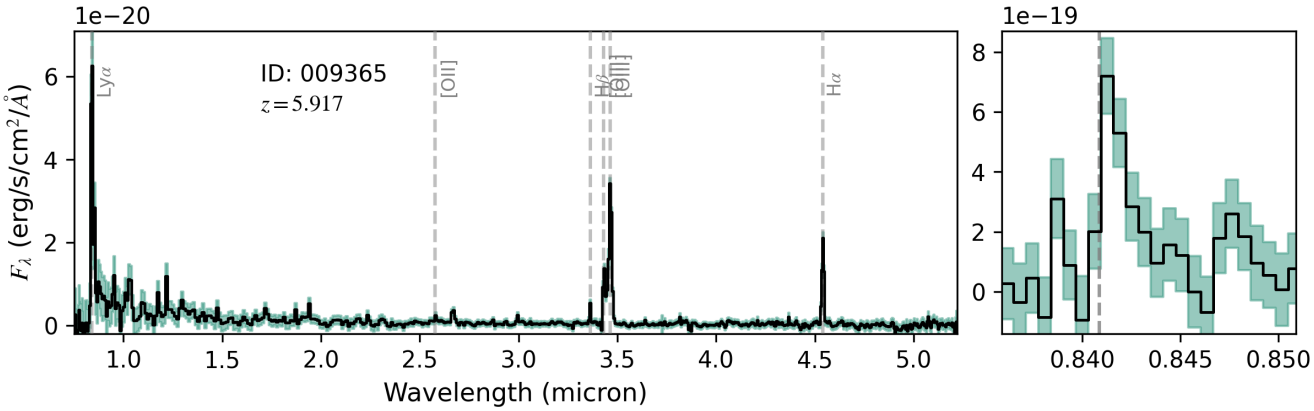

Fig. A.1. continued.